

**A NEW NARROW BAND MICROSTRIP PATCH FILTER FOR MODERN  
WIRELESS APPLICATIONS**

**A THESIS SUBMITTED TO  
THE GRADUATE SCHOOL OF NATURAL AND APPLIED  
SCIENCES OF  
ÇANKAYA UNIVERSITY**

**BY  
ALI NAJDET NASRET CORAN**

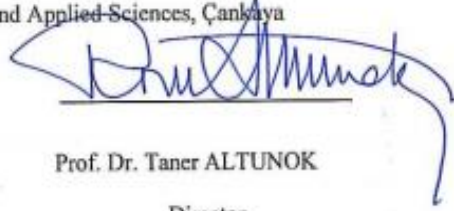
**IN PARTIAL FULFILMENT OF THE REQUIREMENTS THE DEGREE OF  
MASTER  
IN  
THE DEPARTMENT OF  
ELECTRONIC AND COMMUNICATION ENGINEERING**

**JUNE 2014**

**Title of the Thesis: A New Narrow Band Microstrip Patch Filter for Modern  
Wireless Applications**

Submitted by **Ali Najdet Nasret CORAN**

Approval of the Graduate School of Natural and Applied Sciences, Çankaya  
University.



Prof. Dr. Taner ALTUNOK

Director

I certify that this thesis satisfies all the requirements as a thesis for degree of  
Master Science.



Prof. Dr. Celal Zaim ÇIL

Head of Department

This is to certify that we have read this thesis and that in our opinion it is fully  
adequate, in scope and quality as a thesis for the degree of Master Science.



Prof. Dr. Yusuf Ziya UMUL

Supervisor

**Examination Date: 10.06.2014**

**Examining Committee Members**

Prof. Dr. Yusuf Ziya UMUL

(Çankaya Univ.)

Assist.Prof. Nursel AKÇAM

(Gazi Univ.)

Dr. H. Deniz BAŞDEMİR

(Çankaya Univ.)



### STATEMENT OF NON-PLAGIARISM PAGE

I hereby declare that all information in this document has been obtained and presented in accordance with academic rules and ethical conduct. I also declare that, as required by these rules and conduct, I have fully cited and referenced all material and results that are not original to this work.

Name, Last Name : Ali Najdet Nasret CORAN

Signature :



Date

: 10.06.2014

## **ABSTRACT**

### **A NEW NARROW BAND MICROSTRIP PATCH FILTER FOR MODERN WIRELESS APPLICATIONS**

CORAN, Ali Najdet Nasret

M.Sc., Department of Electronic and Communication Engineering

Supervisor: Prof. Dr. Yusuf Ziya UMUL

June 2014, 59 Pages

A narrowband, compact, and flexible fabricated microstrip bandpass filter design is introduced in this thesis as a candidate for use in modern wireless systems. The proposed filter design is based on the use of dual-mode (two pole) patch microstrip resonator with uniform geometrical slot. This filter has the advantages of possessing much narrower and sharper performance responses as compared to single mode resonator and other conventional square patch filters. The performance of filter structures, based on dual-mode resonators, has been evaluated using Microwave office electromagnetic software package. Dual slotted patch microstrip filters have been designed at resonant frequencies 4.16 and 2.04 GHz using a substrate with a dielectric constant of 10.8 and thickness of 1.27mm. Performance simulation results show that these filter structures offer very good frequency responses in addition to narrow bands gained, compactness properties and 2<sup>nd</sup> harmonic isolation in out of band region.

**Keywords:** Microstrip Filter, Patch Bandpass Filter, Narrow Bandpass Filter

## ÖZ

### MODERN KABLOSUZ UYGULAMALAR İÇİN YENİ BİR DAR BANDLI MİKROŞERİT YAMA FİLTRESİ

CORAN, Ali Najdet Nasret

Yüksek Lisans, Elektronik ve Haberleşme Mühendisliği Anabilim Dalı

Tez Yöneticisi: Prof. Dr. Yusuf Ziya UMUL

Haziran 2014, 59 Sayfa

Bu tezde modern kablosuz sistemlerde kullanmak için aday olarak darbandlı, kompakt ve esnek üretilen mikroşerit band geçiren bir filtre tasarımı sunulmuştur. Önerilen filtre tasarımı sürekli geometrik kesitle birlikte çift mod (iki kutup) yama mikroşerit rezonatör kullanımına dayanmaktadır. Bu filtre, tek modlu rezonatör ve diğer geleneksel kare yama filtreler ile karşılaştırıldığında çok dar ve keskin performans yanıtlarına sahip olarak avantajlara sahiptir. Filtre yapısının performansı, çift modlu rezonatöre dayanarak, mikrodalga ofis elektromanyetik yazılım paketi kullanılarak değerlendirilmiştir. Çift yarıkli yama mikroşerit filtreler, dielektrik sabiti 10.8 ve kalınlığı 1.27mm olan dolgu maddesi kullanılarak 4.16 ve 2.04GHz rezonans frekanslarında dizayn edilmişlerdir. Performans simulasyon sonuçları gösterir ki dar band kazancına, sıklık özelliklerine ve band bölgesinin dışında ikinci harmonik izolasyonuna ek olarak bu filtre yapıları çok iyi frekans tepkileri öngörmektedir.

**Anahtar kelimeler:** Mikroşerit Yama Filtre , Band Geçiren Filtre, Dar Bant Geçiren Filtre

## **ACKNOWLEDGEMENTS**

First and foremost, I would like to praise the lord for all the blessings and opportunities bestowed upon me. I would like to express my sincere gratitude and deep appreciation to my advisor Prof.Dr Yusuf Ziya Umul for his unlimited guidance, assistance, encouragement and tremendous patience until finishing this research. I also extend my scincere special thanks to Ph.D student Yaqeen Sabah Mezaal for his objective guidance and firm support. Also, I must not forget to thank Çankaya University, and especially the Department of Electronic and Communication Engineering, for their precious encouragement and facilities. I am very grateful to my parents, my brother Aqeel and my sister Naba for their encouragement and support as this research achieved.

## TABLE OF CONTENTS

STATEMENT OF NON PLAGIARISM.....	iii
ABSTRACT.....	iv
ÖZ.....	v
ACKNOWLEDGMENTS.....	vi
TABLE OF CONTENTS.....	vii
LIST OF TABLES.....	ix
LIST OF FIGURES.....	x
LIST OF ABBREVIATIONS.....	xiii
LIST OF SYMBOLS.....	xiv

### CHAPTERS:

#### 1. INTRODUCTION

1.1. Background.....	1
1.2. The Literature Survey.....	2
1.3. Aim of the Thesis.....	5
1.4. Thesis Outline.....	5

#### 2. MICROWAVE FILTERS: BASICS & CONSEPTS

2.1. Introduction.....	7
2.2. LowPass Prototype Filters.....	8
2.3. Lumped-Element Practical Bandpass Filters.....	12
2.4. Practical Filters with Admittance Inverters.....	14
2.5. The Microstrip Line.....	19
2.6. Unloaded Quality Factor.....	22
2.7. Microstrip Coupled Lines.....	25

<b>3. DUAL-MODE SQUARE PATCH RESONATOR</b>	
<b>3.1. Miniature Dual-Mode Resonator Filters.....</b>	29
<b>3.2. Microstrip Dual-Mode Resonators.....</b>	29
<b>3.2.1. Dual-Mode Resonators.....</b>	32
<b>3.3. Analysis of Dual-Mode Resonator.....</b>	33
<b>3.3.1. Analysis of Odd Mode.....</b>	34
<b>3.3.2. Analysis of Even Mode.....</b>	36
<b>3.4. Equivalent Electrical Model.....</b>	40
<b>4. DESIGN AND SIMULATION OF SLOTTED PATCH MICROSTRIP BANDPASS FILTER</b>	
<b>4.1. Introduction.....</b>	44
<b>4.2. Design and Simulation Results of Slotted Patch Resonator Bandpass Filter.....</b>	44
<b>4.2.1. Design and Simulation Results of BPF Designed for 4.16 GHz... 45</b>	
<b>4.2.2. Design and Simulation Results of BPF Designed for 2.042 and 2.046 GHz Resonant Frequencies.....</b>	49
<b>4.3. Discussion of the Results.....</b>	51
<b>5. CONCLUSIONS</b>	
<b>5.1. Conclusions.....</b>	58
<b>5.2. Suggestions for Future Works.....</b>	58
REFERENCES.....	R1
APPENDIX.....	A1
<b>A. CURRICULUM VITAE.....</b>	A1



## LIST OF TABLES

### TABLES

- Table 1** Summary of the calculated and simulation results of the modeled filter.... 48
- Table 2** Summary of the calculated and simulation results of the modeled filter.... 51

## LIST OF FIGURES

### FIGURES

<b>Figure 1</b>	Two-port microwave filter characterized by reflection and transmission coefficients.....	8
<b>Figure 2</b>	Four categories of ideal frequency selective characteristics.....	9
<b>Figure 3</b>	Frequency-dependent attenuation responses of the third order low-pass prototype.....	10
<b>Figure 4</b>	Lumped element ladder networks of the two types of lowpass prototype filters.....	11
<b>Figure 5</b>	Ladder network of the bandpass microwave filter.....	13
<b>Figure 6</b>	Frequency-dependent attenuation response of the bandpass microwave filter.....	13
<b>Figure 7</b>	Block diagram of (a) impedance inverter and (b) admittance inverter.....	15
<b>Figure 8</b>	Equivalent transformation between the shunt susceptance and series reactance using inverter elements: (a) impedance inverter; (b) admittance inverter.....	16
<b>Figure 9</b>	Equivalent diagrams of lumped-element microwave bandpass filters.....	17
<b>Figure 10</b>	Lumped-element impedance and admittance inverters.....	18
<b>Figure 11</b>	Two bandpass filter prototypes.....	18
<b>Figure 12</b>	Side view of excited microstrip line with corresponding electric and magnetic fields.....	19
<b>Figure 13</b>	Transmission of normalized Chebyshev bandpass filter.....	23
<b>Figure 14</b>	Unloaded Q factor of microstrip $\lambda/2$ resonator for various characteristic impedances.....	24

## FIGURES

<b>Figure 15</b>	Comparison of 5 <sup>th</sup> order Chebyshev filter transmission response.....	25
<b>Figure 16</b>	Side on view of field distribution of microstrip coupled lines.....	26
<b>Figure 17</b>	Lumped element circuit model of coupled transmission.....	27
<b>Figure 18</b>	(a) Cavity model of a dual-mode microstrip resonator. (b) Equivalent circuit of the dual-mode resonator.....	30
<b>Figure 19</b>	Some microstrip dual-mode resonators.....	31
<b>Figure 20</b>	Basic layout of dual-mode resonator.....	33
<b>Figure 21</b>	Odd mode resonator configuration .....	34
<b>Figure 22</b>	(a) Voltage and current distribution along odd mode resonator normalised to the resonator length, where $Z_1 = 1$ (b) Full wave EM simulated charge distribution along dual mode resonator (c) Full wave EM simulated current distribution along dual-mode resonator.....	36
<b>Figure 23</b>	Even mode resonator configuration .....	37
<b>Figure 24</b>	Supported fundamental resonant guided wavelength of even mode, normalized to the first order odd mode guided wavelength, plotted against the length of line 2 expressed as a percentage of that of line 1 for various impedance ratios $Z_{2e}/Z_1$ .....	38
<b>Figure 25</b>	(a) Voltage and current distribution along even mode resonator normalised to the resonator length (b) Full wave EM simulated charge distribution along dual-mode resonator (c) Full wave EM simulated current distribution in the x direction (d) Full wave EM simulated current distribution in the y direction.....	40
<b>Figure 26</b>	(a) (b) Equivalent circuits of the dual-mode resonator (c) Dual-mode resonator with extracted impedance inverter.....	42
<b>Figure 27</b>	The layout of the modeled dual-mode slotted patch BPF.....	45

## FIGURES

<b>Figure 28</b>	Flow chart for Moore BPF design.....	46
<b>Figure 29</b>	The return loss and transmission responses of proposed BPF designed for 4.16 GHz.....	47
<b>Figure 30</b>	The phase responses of proposed slotted patch BPF.....	48
<b>Figure 31</b>	The return loss and transmission responses of proposed BPF designed for 2.04 GHz resonant frequencies.....	49
<b>Figure 32</b>	The phase responses of proposed slotted patch BPF.....	50
<b>Figure 33</b>	The layout of the modeled dual-mode conventional patch BPF.....	53
<b>Figure 34</b>	The transmission responses of the two filters; with and without uniform slot at 4.16 and 5.77 GHz respectively.....	53
<b>Figure 35</b>	The return loss responses of the two filters; with and without uniform slot at 4.16 and 5.77 GHz respectively.....	54
<b>Figure 36</b>	The out-of-band transmission responses of the proposed filter designed for 4.16 GHz fundamental frequency.....	54
<b>Figure 37</b>	The out-of-band transmission responses of the proposed filter designed for 2.04 GHz fundamental frequency.....	55
<b>Figure 38</b>	Simulated current density distributions of the proposed BPF at 4.16 GHz fundamental frequency (in passband region).....	55
<b>Figure 39</b>	Simulated current density distributions of the proposed BPF at 2.04GHz fundamental frequency (in passband region).....	56
<b>Figure 40</b>	Simulated transmission responses, S21, of proposed BPF as a function of d in units of mm for the case of 4.16 GHz.....	56
<b>Figure 41</b>	Simulated transmission responses, S21, of proposed BPF as a function of d in units of mm for the case of 2.04 GHz.....	57

## **LIST OF ABBREVIATIONS**

<b>BPF</b>	<b>BandPass Filter</b>
<b>CSRR</b>	<b>Complement Split-Ring Resonator</b>
<b>TEM</b>	<b>Transverse Electromagnetic</b>
<b>FBW</b>	<b>Frequency Band Width</b>
<b>FDTD</b>	<b>Finite Difference Time Domain</b>

## LIST OF SYMBOLS

$\Omega$	Angular Frequency
$Z_s$	Internal Impedance
$R(\omega)$	Reflection Coefficients
$T(\omega)$	Transmission Coefficients
$\omega_c$	Cut Off Frequency
$V_p$	Phase Velocity
$T$	Conductor Thickness
$H$	Substrate Height
$W$	Line Width
$R_s$	Surface Resistance
$\alpha_c$	Attenuation Constant
$L_i$	Mid-Band Insertion Loss
$Q_{ui}$	Resonator
$N$	Filter Order
$g_i$	Lowpass Prototype Element Values
$\epsilon_r$	Relative Permittivity
$L_m$	Mutual Inductance
$C_m$	Mutual Capacitance
$\gamma$	Wavelength
$K_e$	Electric Coupling Coefficient
$K_m$	Magnetic Coupling Coefficient
$\gamma_{go}$	Guided-Wavelength
$I(x)$	Current Distribution
$X_r$	Reactance Slope
$C_s$	Series Capacitance
$X_s$	Susceptance Slope
$C_p$	Resonator Capacitance
$Z_{sc}$	Short Circuited Stub

## CHAPTER 1

### INTRODUCTION

#### 1.1. Background

Promising wireless communication systems must have variety of systems with multi-band and multifunctional properties. Currently, RF and microwave filters have affected by a normal development by applying tunability to their passive functions. A microstrip bandpass filter scan be easily mounted and the circuit layout design can be more flexible[1]. The dual-mode resonators were popular for many years ago. The miniaturized and efficient microwave bandpass filters are hugely requested in the wireless communications systems because of their advantages such as small size, low loss, light weight and high selectivity. Many wide-band bandpass filters have been proposed using dual-mode ring resonators with tuning stubs but their topologies still take a big circuit area, which is not appropriate for wireless communication systems in which the compactness parameter is very important factor [2], [3]. It is popular to build up new types of dual-mode microstrip resonators not only for giving different designs, but also for reducing the size of filters. On the other hand, the recent wireless communication systems necessitate the bandpass filters having useful out-of-band spurious rejection and good in-band performance. Therefore, the resonators are broadly used in design of antennas [4] and filters [5], [6]. Microstrip bandpass filters have been widely used in a variety of microwave circuits and systems. Recently, the dual-mode concept means two degenerate modes of a geometrically symmetrical resonator, and its main feature and advantage is that each dual mode resonator can be used as a doubly tuned resonant circuit, which considers as compact filter configuration [3][5]. For dual mode operation, a perturbation with an asymmetrical supply line resonator element or an exciting two degenerate resonant modes must be introduced to split and double. Microstrip dual-mode bandpass filter may be square patch [3], circular patch, triangular patch [3,4,7], trapezoidal patch and their ring patches [8], et al., and can be made-up by direct coupling without coupling gaps.

In this dissertation microstrip slotted patch band pass filter with narrow band responses and adequate performances has been presented.

## 1.2. The Literature Survey

In 2002, B. T. Tan, et al. [9], proposed a circular holes that are etched off of a microstrip disk resonator. This results in a reduction of 30% in size. By compensating for some of these holes by location and putting the other degenerate excited, a split-mode bandpass filter will be resulted . This filter can be as a lattice-type structure. A filter with a bandwidth of 8% centered at 2.0 GHz was designed. Insertion loss measurement 0.6 dB. The filter is fabricated on substrate  $\epsilon_r = 10.2$  and thickness 25 mm.

In 2003, X. Wang, Y. Li [10], displayed new microstrip triangular patch resonator filters with two transmission zeros. The filters have been demonstrated by simulation and measurement with good agreement. These filters are fabricated on substrate  $\epsilon_r = 10.8$  and thickness 0.635mm.

In 2004, O. Akgün, et al. [11], proposed compact and low-loss resonator loaded with two narrow openings changer dual-mode debugging narrow filter using degenerate modes changer. Two adjacent edges of the slot and the patch modulator connected directly to the center line of the structure of the resonator is fed additional .The filter is fabricated on substrate with  $\epsilon_r = 10.2$  and thickness 1.27 mm.

In 2005 C. Lugo Jr. and J. Papapolymerou[12], proposed a reconfigurable bandpass filter using a dual-mode microstrip triangular patch resonator. The proposed circuit uses a single switch to control its fractional bandwidth while keeping a fixed center frequency of 10 GHz. The switching mechanism is accomplished by a p-i-n diode that connects and isolates a tuning stub from the rest of the circuit. The on and off state of the diode effectively controls the resonance frequencies of the two poles produced by the dual-mode behavior of the resonator. The filter achieves a measured 1.9:1 tunable passband ratio. The circuit presented here represents the first single switch bandwidth reconfigurable filter that requires no size compensation to maintain



a fixed center frequency. The filter is modeled on a substrate  $\epsilon_r = 10.2$  and thickness 25mils.

In 2006 A. F. Sheta, et.al [13], introduced a new non-degenerate dual-mode microstrip. The proposal is based on the candidate in the form of a symmetrical four slot etched minute patch on the form. In addition to its simple structure, the filter has the advantages of small size and low loss. The finite difference time domain (FDTD) method is used to analyze the proposed structure. The filter is fabricated on substrate with  $\epsilon_r = 10.8$  and thickness 0.635 mm.

In 2007 C.H. Chen, et.al [14], proposed dual compact dual-mode equilateral triangular patch filters with an inverted T-shaped slot and an inverted H-shaped slot were intended and fabricated. As the same as equilateral triangular patch resonator, the inverted T-shaped and inverted H-shaped slots perturb the primary mode and lower the resonant frequency, which lessen the related size. The triangular patch structure with inverted T-shaped and inverted H-shaped slots loading have size reduction of 12.4% and 27.5%, respectively, at the same centre frequency compared with the original equilateral triangular patch resonator. The filter is designed on a  $\epsilon_r = 9.8$  and thickness 1.0 mm.

In 2008 Y. K. Singh and A. Chakrabarty [15], displayed two slots oriented orthogonal to each other which are cut on a circular patch resonator. The slots bring down the fundamental resonance frequency of the patch. The second higher order mode, however, remains unaffected. This effectively miniaturizes the patch by 57.8% at the same time increases the harmonic separation by 2.51 times. By adding two more slots parallel to and on both the sides of each arm of the crossed slot, fundamental frequency can be further brought down resulting in a filter which is 87.4% smaller compared to a circular patch. The second passband appears at a frequency which is 4.66 times that of the first passband center frequency. The filter is fabricated on a substrate with  $\epsilon_r = 4.3$  and thickness 1.5875 mm.

In 2009 B. K. Esfeh [16], A narrowband bandpass filter using dual-mode microstrip square loop resonator is proposed. This structure has a 5.1% fractional bandwidth at 2.3GHz. By using some simple techniques, the optimum results will be achieved. The dual-mode resonator will be produced by adding a square patch inside the loop

resonator. The filter is fabricated on RT/Duroid 6010 substrate having a relative dielectric constant of 10.2 and 0.635 mm thickness. The final dimension is measured at 19.65 mm× 19.65 mm. The minimum measured insertion loss is 1.68 dB and return loss obtained is better than -20 dB, where the experimental results and simulated values are in good agreement.

In 2011 Y. C. Li [17], developed a dual-mode dual-band bandpass filter using a patch resonator with a cross slot and two different groups of stubs loaded. The cross slot with different orthogonal lengths excites orthogonal modes in the passbands and reduces the patch size. Meanwhile, the two sets of stubs can modify the filter's input impedance at different frequencies and control the even and odd modes in the passbands, respectively. Utilizing these two kinds of elements, transmission poles can be realized easily in both passbands. For demonstration, a dual-band patch resonator filter working at 2.4 and 5.2 GHz designed. The filter is fabricated on a substrate with  $\epsilon_r = 10.2$  and thickness 1.27 mm.

In 2012 R. Zhang and L. Zhu, [18], microstrip bandpass filters using a triple-mode patch-loaded cross resonator are presented. Firstly, a square patch is added at the center of a cross resonator to separate the resonant frequencies of the 1<sup>st</sup> and 2<sup>nd</sup> modes. Then, a pair of narrow slots is etched into the square patch along its symmetrical plane to split the 1<sup>st</sup> resonant mode and its degenerate mode. By changing the patch size and the slot length, the above three modes are appropriately adjusted. Two prototype filters with open-ended and stub-loaded coupled-lines are designed and fabricated to verify the design principle and to further suppress the lowest harmonic passband, respectively. Predicted results agree well with the measured ones.

In 2013 R. Zhang, et al.[19], A class of microstrip triple-mode Bandpass Filters (BPFs) using a patch-loaded cross resonator are modeled, designed and tested. First, a symmetrical equivalent LC network is developed for a symmetrical patch structure. The values of all the inductors and the capacitors are extracted by applying the even-odd mode analysis. Then, three 1-port networks are developed to analyze the resonant conditions of the corresponding modes. Finally, these first three resonant modes are used to form a passband with three transmission poles. To verify the

proposed design methodology, two sets of filter prototypes with different loaded patches are designed, fabricated and measured in the end. The predicted results are well confirmed with the experimental ones. The filter is fabricated on a substrate with  $\epsilon_r = 10.2$  and thickness 1.27 mm.

In 2014 X. Liua, X. Shib [20], A compact dual-mode microstrip bandpass filter using square-patch resonator and a new perturbation element is designed. This new slot-type element is composed by a complement split-ring resonator (CSRR) with two pairs of etching slots. The nature of coupling between the degenerate modes is investigated with respect to the perturbation size. By proper arranging the orientations of the CSRRs, new coupling characteristics can be obtained. The filter is modeled on a substrate with  $\epsilon_r = 3.48$  and thickness 0.762 mm.

### **1.3. Aim of the Thesis**

The main goal of this thesis is to introduce miniaturized microstrip bandpass filter design structure for modern wireless communication applications. The proposed filter design consists of dual mode slotted square patch which has been modeled, simulated and evaluated using EM simulator Microwave Office 2009. For the following purposes:

- 1-Compact Size.
- 2-Narrowband responses
- 3-Flexibility Design .
- 4-Harmonics suppressions.

### **1.4. Thesis Outline**

This thesis is organized as follows :

- Chapter one presents the background and literature survey of microstrip patch bandpass filters .
- Chapter two includes the basics of microstrip bandpass filters as well as their properties and applications.
- Chapter three shows the fundamentals of dual-mode square patch resonator.

- Chapter four contains design and simulation results of proposed model of microstrip filter.
- Chapter five includes the conclusions and the recommendations for future work.

## CHAPTER 2

### MICROWAVE FILTERS: BASICS& CONCEPTS

#### 2.1. Introduction

Microwave filters [21] and [22] are the basic building blocks with frequency-selective or filtering functionality in the development of various wireless systems that operate at frequency ranges above 300 MHz. Filter blocks play a key role in effectively transmitting the desired signals in certain pass-band regions while attenuating all the undesired signals in the remaining band-stop regions. Basically, microwave filters can be classified into four distinct categories: low-pass, high-pass, band-pass, and band-stop filter blocks [21]. The first two types of blocks realize effective transmission in the entire frequency region below or above a cutoff frequency while the third and fourth types transmit or attenuate signals within a certain frequency region that is terminated by the lower and upper cutoff frequencies. At low frequencies, lumped-element capacitors and inductors can be reasonably constructed to structure all the filters classified above on the basis of efficient synthesis approach [21]. However, as the operating frequency increases to the microwave region of interest, the reactance or susceptance of all the microwave circuit elements, including the supposed lumped elements, varies as a nonlinear function of frequency. Therefore, the design of microwave filters should account for the distributed nature of a variety of microwave circuit elements. These elements can still be approximated as quasi-lumped elements in the low- or narrow band frequency region. As a result, the early developed synthesis procedure still can be effectively executed in the microwave range to efficiently design the microwave filters with acceptable accuracy in the frequency region of interest [23].

## 2.2. LowPass Prototype Filters

Fig.1 depicts the schematic of a general two-port filter that is driven by a voltage source ( $V_s$ ) with the internal impedance ( $Z_s$ ) and terminated by the load impedance ( $Z_L$ ). Under the assumption that the incident wave has the unity amplitude, the amplitudes of the reflected and transmitted waves are referred as the reflection and transmission coefficients, namely,  $R(\omega)$  and  $T(\omega)$  ( $\omega$  = angular frequency), which are frequency-dependent in a complex mode in conjunction with the varied pass-bandstop-band characteristics.

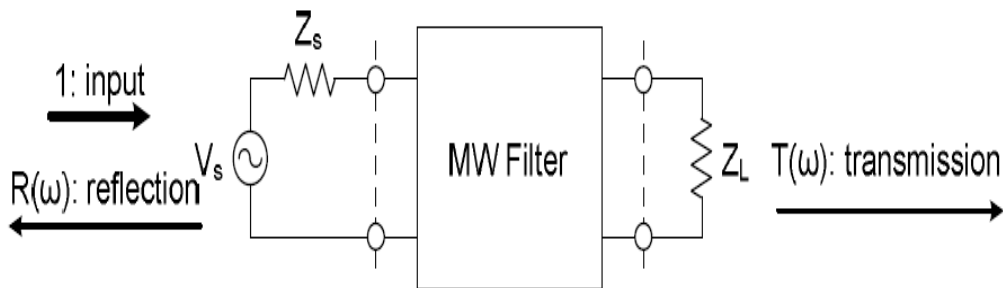


Figure 1: Two-port microwave filter characterized by reflection and transmission coefficients:  $R(\omega)$  and  $T(\omega)$ .

Fig.2 illustrates the frequency responses of the four categories of ideal filters with perfect transmission in the pass-band and infinite attenuation in the stop-band,  $T(\omega) = 1$  and  $T(\omega) = 0$ , respectively. As seen in Figures 2.a and 2.b, low-pass filters transmit all signals below the cutoff frequency ( $\omega_c$ ) and reject those above  $\omega_c$  while the high-pass filters attenuate all signals below  $\omega_c$  and pass those above ( $\omega_c$ ). On the other hand, the ideal bandpass and bandstop filters perfectly pass and attenuate all frequencies in the range of lower and upper cutoff frequencies,  $\omega_{c1}$  and  $\omega_{c2}$ , as shown in Figures 2.c and 2.d.

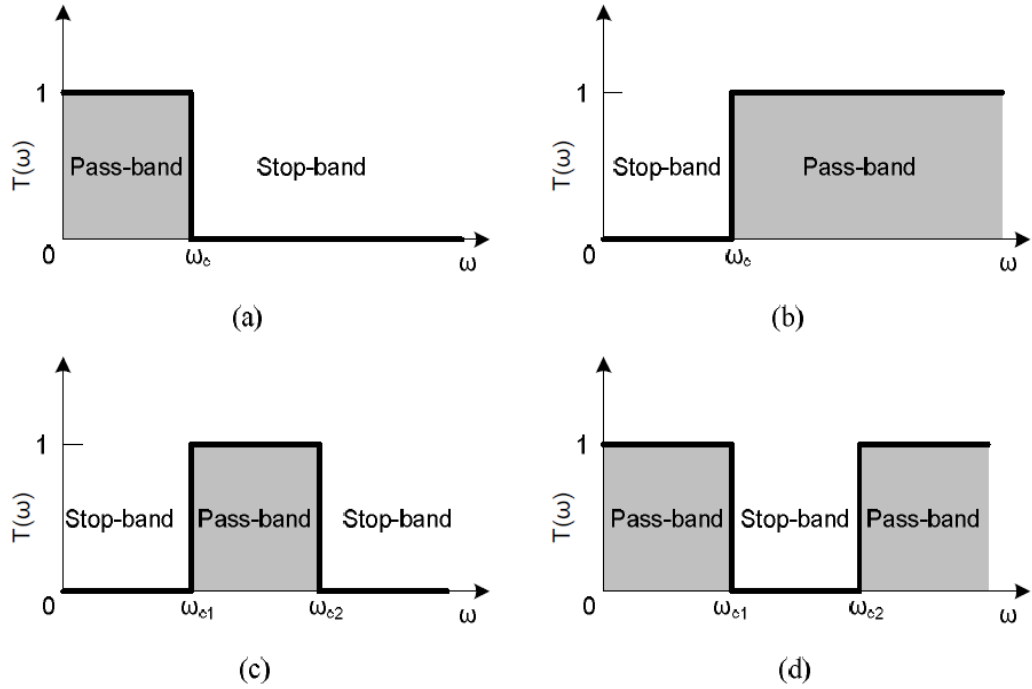


Figure 2: Four categories of ideal frequency selective characteristics:(a) low-pass filter; (b) high-pass filter; (c) band-pass filter; (d) band-stop filter.

The low-pass prototype filter may be characterized in the normalized frequency  $\Omega = \omega / \omega_c$ , where  $\omega_c$  is the cutoff frequency, and its frequency response is specified under the power insertion loss parameter:  $L(\Omega) = 1 / |T(\Omega)|^2$ , Furthermore,  $L(\Omega)$  is expressed in terms of a general polynomial function  $FN(\Omega)$ , where  $N$  is the order of the low pass filter, such that [24]

$$L(\Omega) = 1 + k^2 FN(\Omega) \quad (2.1)$$

where  $k$  is the constant related to the ripple or tolerance within the passband. Selection of  $FN(\Omega)$  should be based on the condition that the network topology can be physically constructed. In this situation, two essential forms can be specified in the practical implementation: maximally flat or Butterworth filters and Chebyshev or equal-ripple filters. Equations (2.2) to (2.5) indicate their insertion loss parameters as a function of  $\Omega$ , respectively, in which  $TN(\Omega)$  is the  $N$ th-order Chebyshev function [24]. For Butterworth filter, the insertion loss parameter is

$$L(\Omega) = 1 + k^2 \Omega^{2N} \quad (2.2)$$

and for Chebyshev filter, the insertion loss parameter is

$$L(\Omega) = 1 + k^2 T_N^2(\Omega) \quad (2.3)$$

Figures 3.a and 3.b show the frequency responses of the decibel insertion losses  $L$  (dB) of the third-order low-pass prototype filters with  $N = 3$ . In order to quantitatively evaluate their low-pass characteristics, the insertion loss at the cutoff frequency

( $\Omega_c = 1$ ) is specified as  $L_c$ . Looking at these two curves together, one can easily find that the Chebyshev filter increases much more rapidly beyond  $\Omega_c$  in comparison to its Butterworth equivalent. In other words, the Chebyshev one has a much sharper cutoff

frequency region separating the lower and higher stop-bands, which is preferably desired to approach the ideal frequency response as shown in Figure 2a.

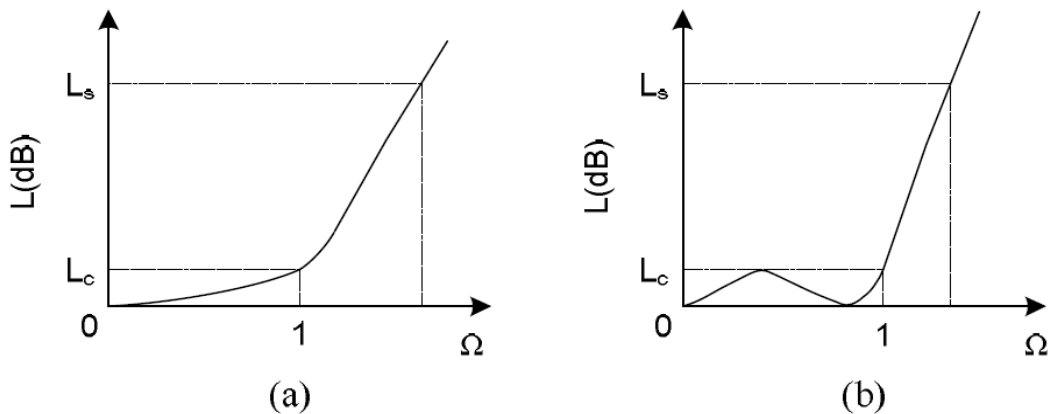


Figure 3: Frequency-dependent attenuation responses of the third order low-pass prototype filters: (a) Butterworth type; (b) Chebyshev type

Figures 4.a and 4.b depict the ladder networks of the two possible low-pass prototype filters, in which the element  $g_k$  is the  $k^{\text{th}}$  normalized inductance or capacitance while  $g_0$  and  $g_{N+1}$  are the normalized source and load resistance or conductance at the input and output ports, respectively. Their input impedances are first derived and then converted to their relevant insertion loss. As such, the values of each elements  $g_k$  ( $k = 1, 2, \dots, N$ ) for the load  $g_{N+1}$  can be analytically calculated under the exact equality of the two sets of insertion loss, given in Equations (2.2) and (2.3), and derived from the ladder networks in Figure 4. For the Butterworth low-pass



prototype filter with  $L_c = 3\text{dB}$  at  $\Omega_c = 1$  in which  $k = 1$ , the element values ( $g_k$ ) may be calculated in the following closed-form equations:

$$g_0 = g_{N+1} = 1 \quad (2.4)$$

$$g_k = 2 \sin \left[ \frac{2k-1}{2N} \pi \right] = 1, 2, \dots, N \quad (2.5)$$

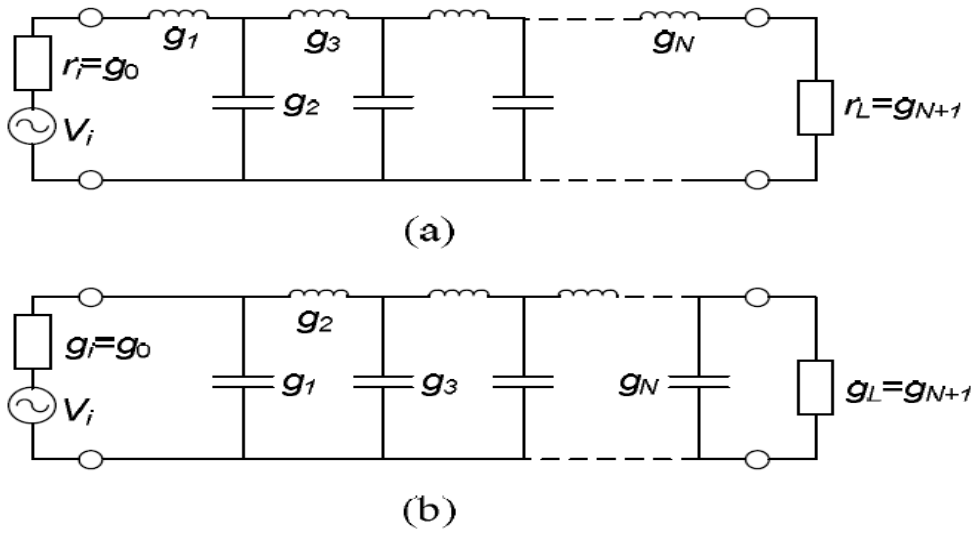


Figure 4: Lumped-element ladder networks of the two types of lowpass prototype filters: (a) inductive type; (b) capacitive type.

For the Chebyshev prototype filter with the required insertion loss  $L_c$  at  $\Omega_c = 1$ , the constant  $k$  can be determined from Equation (2.3):  $L_c = 10 \log(1 + k^2)$ . For instance, if  $L_c = 0.1$  dB, which is the equal ripple in the low pass-band, one can obtain

$k = 0.153$ . Next, the values of each element  $g_k$  can be derived for the given  $N$  using Equations (2.6), (2.7) and (2.8), respectively. Selection of the integer number  $N$  should be based on the required stop-band performance that can be specified by the insertion loss ( $L_s$ ) at the frequency  $\Omega_c$  with reference to Figures 3a and 3b [23].

$$g_1 = \frac{2a_1}{\sin \sinh\left(\frac{\beta}{2N}\right)} \quad (2.6)$$

$$g_k = \left[ \frac{4a_{k-1}a_k}{b_{k-1}g_{k-1}} \right] \quad k = 2, 3, \dots, N \quad (2.7)$$

$$g_{N+1} = \begin{cases} 1 & N \text{ odd} \\ 2K^2 + 1 - 2K\sqrt{1+K^2} & N \text{ even} \end{cases} \quad (2.8)$$

Where

$$\beta = \ln \left[ \frac{\sqrt{1+k^2} + 1}{\sqrt{1+k^2} - 1} \right], \quad a_k = \text{Sin} \left[ \frac{2K-1}{2N} \pi \right]$$

$$b_k = \sinh^2 \frac{\beta}{2N} + \sin^2 \frac{K\pi}{N}$$

### 2.3. Lumped-Element Practical Bandpass Filters

The low-pass prototype filter is characterized above using the normalized source/load resistance or conductance ( $g_0$  and  $g_{n+1}$ ) as well as the normalized susceptance or reactance ( $g_k$ ) of a Nth-order ladder network in the normalized frequency domain

( $\Omega = \omega/\omega_C$ ). In order to apply this approach to design the lumped-element practical low-pass, high-pass, band-pass, and band-stop filters that operate in the real frequency domain ( $\omega$ ), the frequency transformation is required to map a frequency response in the  $\Omega$  domain to that in the  $\omega$  domain. Meanwhile, the impedance scaling procedure should be executed to guarantee the identical insertion loss responses of the low-pass prototype filter and its transformed practical filter. Under this constraint, the normalized prototype elements can be scaled to their relevant resistance/conductance elements at the source and load sides as well as the reactive/susceptive elements of various practical filter networks. In the following, the frequency and element transformations for a bandpass filter are summarized with

reference to the network topology in Figure 5 and its frequency response in Figure 6. The source and load resistances can be commonly assumed ( $g_0 R_i = g_{N+1} R_L$ ) for simplification of theoretical description [23].

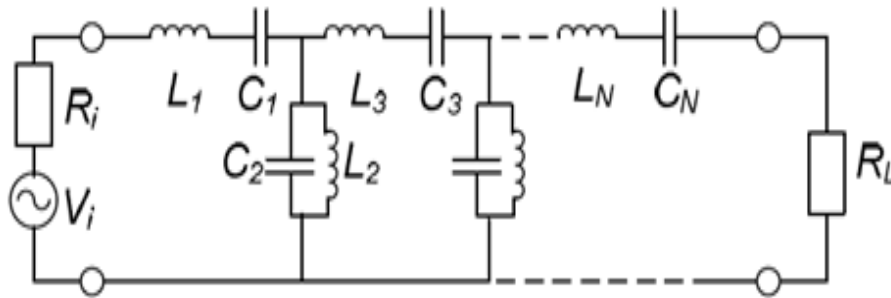


Figure 5: Ladder network of the bandpass microwave filter[23].

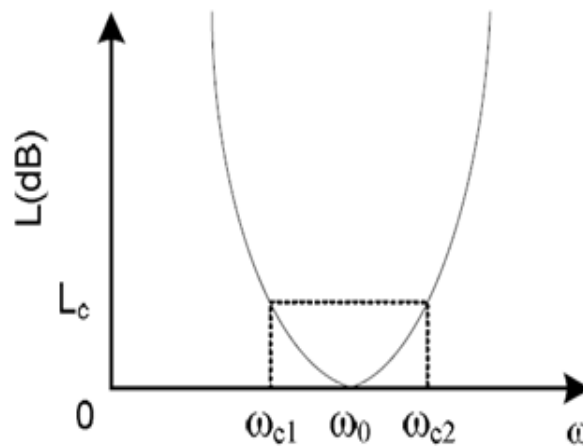


Figure 6: Frequency-dependent attenuation response of the bandpass microwave filter.

To structure the bandpass filter in Fig 5, the frequency transformation should be selected to realize a bandpass response with the pass-band utilizing Equation (2.9). Fig.5 implies that the inductive and capacitive prototype elements should be simultaneously transformed to the series and parallel LC resonators in the bandpass filters.

Under the constraint that the insertion losses (Lc) at the lower/higher cutoff frequencies (i.e.,  $\omega_{c1}$  and  $\omega_{c2}$  in Fig. 6), must be equal to that (Lc) at  $\Omega c = 1$  of its related lowpass prototype filter, the inductance and capacitance,  $L_k$  and  $C_k$ , of each LC resonator are derived by [23]

$$\Omega = \frac{\omega_0}{\omega_{c1} - \omega_{c2}} \left[ \frac{\omega}{\omega_0} - \frac{\omega_0}{\omega} \right] \quad \text{where } \omega_0 = \sqrt{\omega_1 \omega_2} \quad (2.9)$$

$$L_k = \frac{g_k R_L}{\omega_{c1} - \omega_{c2}}, \quad C_k = \frac{\omega_{c2} - \omega_{c1}}{\omega_0^2 g_k R_L} \quad \text{for series Lc} \quad (2.10)$$

$$L_k = \frac{R_L(\omega_{c2} - \omega_{c1})}{\omega_0^2 g_k}, \quad C_k = \frac{g_k}{R_L(\omega_{c2} - \omega_{c1})} \quad \text{for parallel Lc} \quad (2.11)$$

#### 2.4. Practical Filters with Admittance Inverters

The bandpass filter shown in Fig.5 is derived from the low pass filter prototype in Fig.4. The filter consists of series and shunt resonators connected directly without any separation. In the practical implementation, it sometimes seems so difficult, especially in the microwave frequency range, to simultaneously structure both series and parallel LC resonators. As such, the admittance inverter, which is either an impedance or admittance inverter, is utilized to build up an alternative class of filter networks containing only series elements or only parallel elements. Figure 7 depict the two-port impedance and admittance inverters that invert the load impedance  $Z_b$  or admittance  $Y_b$  at one port to the input  $Z_a$  or  $Y_a$  at the other port with respect to the squared characteristic impedance and admittance, namely,  $K$  and  $J$ , respectively [23].

$$Z_a = \frac{K^2}{Z_b}, \quad Y_a = \frac{J^2}{Y_b} \quad (2.12)$$

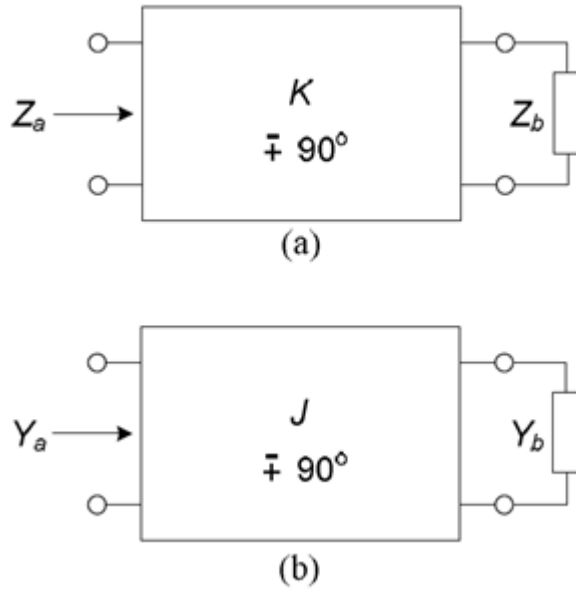


Figure 7: Block diagram of (a) impedance inverter and (b) admittance inverter[23].

Consider the parallel admittance element  $Y_p(\omega)$  sandwiched by the two identical impedance inverters ( $K$ ) at its two sides as shown in Fig 8a. The input impedance, looking into this network from both left and right sides, can be derived as  $K^2 Y_p(\omega)$ , that is, the series impedance  $Z_s(\omega)$ . So, the shunt admittance  $Y_p(\omega)$  can be inverted to the series impedance  $Z_s(\omega)$ . Similarly, the series impedance  $Z_s(\omega)$  with the admittance inverters ( $J$ ) at its two sides is the equivalence of a parallel admittance  $Y_p(\omega)$  as denoted in Figure 8b. The unique feature of these admittance inverters enables us to convert the practical filter blocks in Fig.5 to those with either series or parallel elements. Most importantly, it provides us with much more convenience in the design of microwave bandpass filters with only series or parallel lumped/distributed resonators [23].

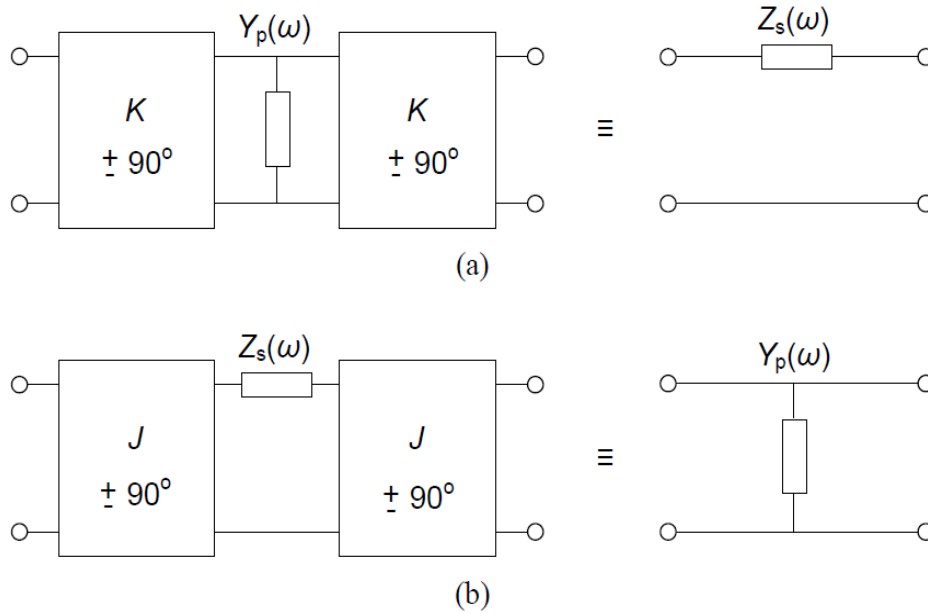


Figure 8: Equivalent transformation between the shunt susceptance and series reactance using inverter elements: (a) impedance inverter; (b) admittance inverter.

Figures 9.a and 9.b describe the two types of bandpass filter networks using the impedance and admittance inverters, respectively. In the former case, only series resonators with the reactance  $X_k(\omega)$  are involved, and the two adjacent ones with  $X_k(\omega)$  and  $X_{k+1}(\omega)$  are cascaded across the impedance inverter,  $K_{k,k+1}(\omega)$ , which is assumed frequency independent. In the latter case, only parallel resonators with the susceptance  $B_k(\omega)$  exist and the admittance inverter  $j_{k,k+1}(\omega)$  is utilized to link the two adjacent resonance susceptances  $B_k(\omega)$  and  $B_{k+1}(\omega)$ . The series or shunt resonators are usually the distributed circuits that are equivalently formulated by various transmission-line and waveguide cavity resonators.

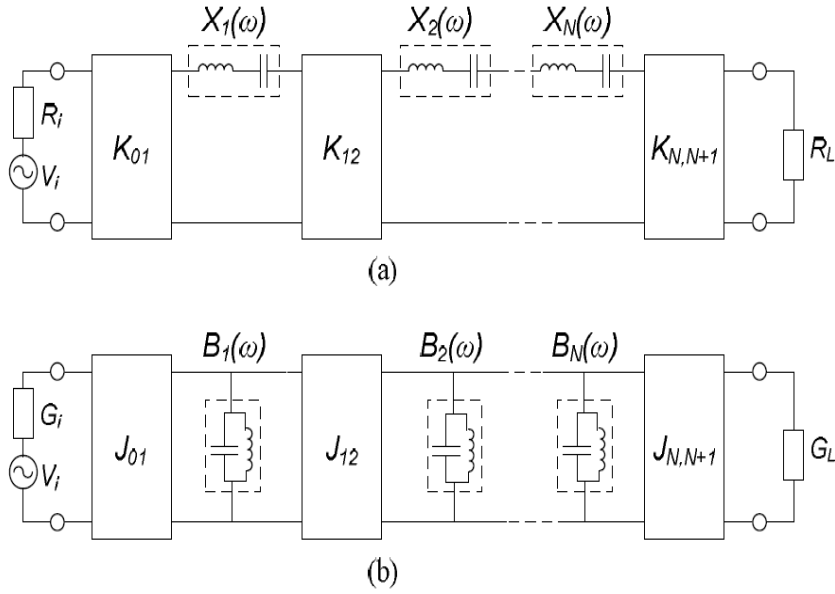


Figure 9: Equivalent diagrams of lumped-element microwave bandpass filters using (a) impedance inverter and (b) admittance inverter.

In the filters with admittance inverters, the impedance and admittance inverters are the two essential circuit elements that could be in practice constructed by the use of quasi-lumped inductors/capacitors at low frequencies, distributed quarter-wavelength transmission lines with lower/higher characteristic impedances, and so on. As shown in Figures 10.a and 10.b, the lumped T network with the positive inductance/capacitance,  $L$  or  $C$ , in shunt and two identical negative ones,  $L$  or  $C$ , in series can structure a simple impedance inverter with the characteristic impedance  $K = \omega_L$  or  $K = 1/\omega_C$ . Similarly, the admittance can be formulated using the lumped  $\pi$  network and its characteristic admittance can be expressed as  $J = 1/\omega_L$  or  $J = \omega_C$ , as also denoted in Figures 10.c and 10.d. The negative  $L$  or  $C$  may be absorbed into adjacent series or parallel resonators so as to eliminate them from the overall filter network in practical design [23].

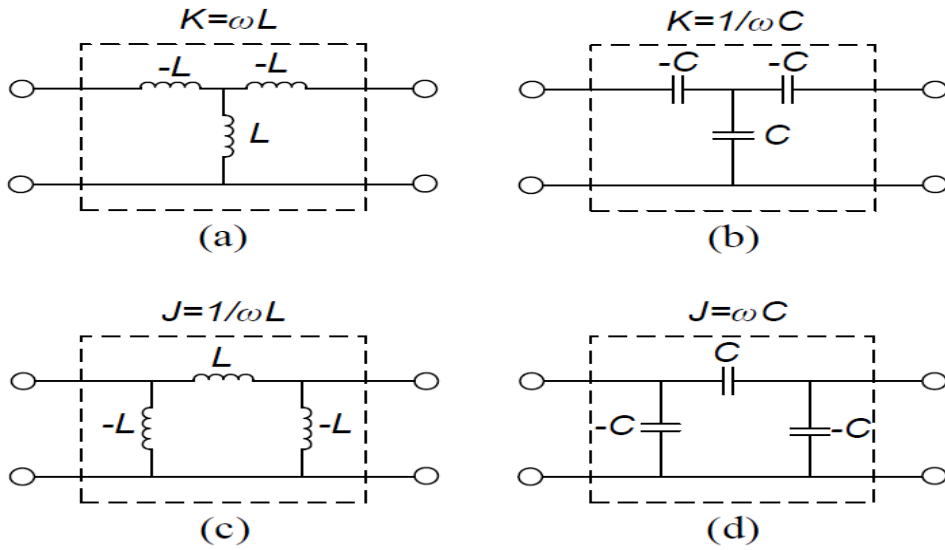


Figure 10: Lumped-element impedance and admittance inverters: (a) inductance T network; (b) capacitance T network; (c) inductance  $\pi$  network; (d) capacitance  $\pi$  network.

Therefore, the most suitable inversion network to choose for a given filter is one whose negative elements can be absorbed into the resonant circuits so that all element values of the composite filter are positive. Figures 11.a and 11.b illustrate the two types of bandpass filter networks after applying lumped-element impedance and admittance inverters shown in Figures 10.a and 10.d, respectively.

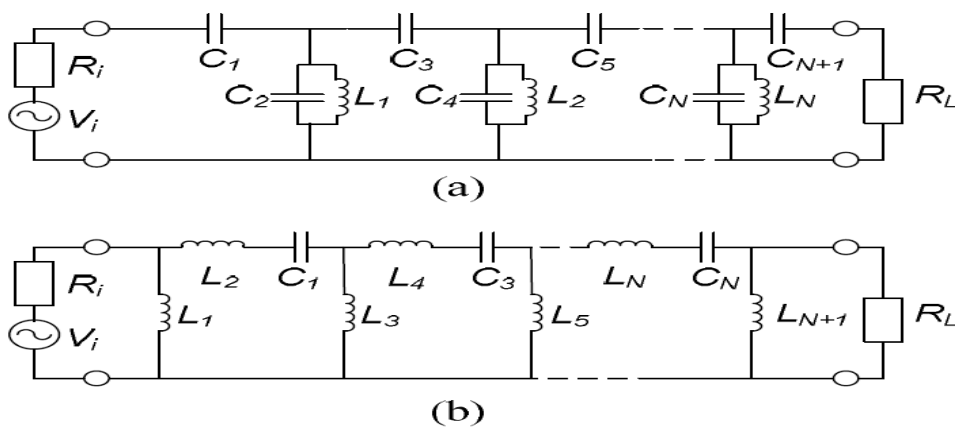


Figure 11: Two bandpass filter prototypes (a) series capacitive coupling using capacitive  $\pi$  network and (b) shunt inductive coupling using inductive T network.



The above two networks represent the prototype bandpass filters for series capacitive, and shunt inductive coupling, respectively.

## 2.5. The Microstrip Line

The microstrip transmission line essentially consists of two conductors separated by some form of dielectric material as illustrated in Fig.12. The top conductor is designated as the signal line while the bottom plate, which is usually several times wider, serves as the ground plane. The properties of these two conductors together with the dielectric filling determine the signal transmission characteristics of the line. Due to the exposed nature of the microstrip line, the electromagnetic fields exist not only within the dielectric but some also extend into the air above. As the relative permittivity of the material  $\epsilon_r$  is almost always greater than unity, the resulting inhomogeneous interface cannot support a pure TEM wave between the air-dielectric interface since the fields in air will invariably propagate faster than the fields within the dielectric.

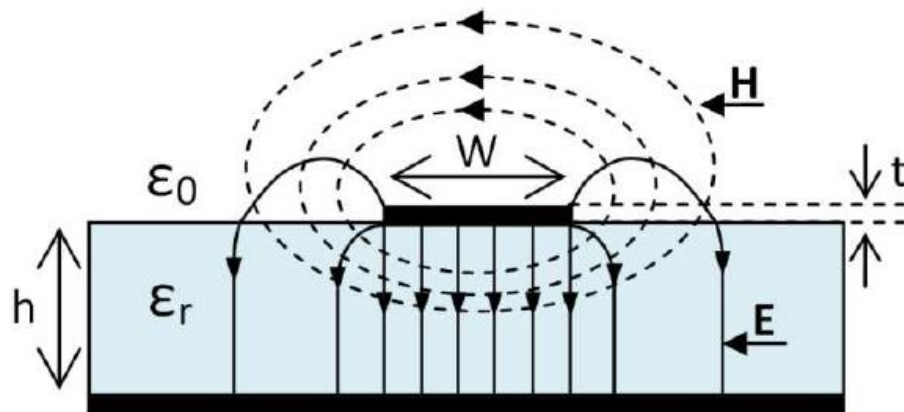


Figure 12: Side on view of excited microstrip line with corresponding electric (solid lines) and magnetic (dashed lines) fields.

The relatively weak longitudinal field components however enable a quasi-static approximation to be employed in characterizing the line up to a few Giga hertz .This approach assumes the propagation of a pure TEM mode which greatly simplifies the related calculations. Once the capacitance per unit length with and without the dielectric,  $C_d$  and  $c_o$  respectively are determined, the effective relative dielectric

constant,  $\epsilon_{\text{eff}}$ , the characteristic impedance,  $Z_0$ , phase constant,  $\beta$ , and phase velocity,  $V_p$ , may be computed using (2.13) - (2.16) respectively, where  $c$  is the speed of light in free space.

$$\epsilon_{\text{eff}} = \frac{C_d}{C_0} \quad (2.13)$$

$$Z_0 = \frac{1}{C\sqrt{C_0 C_d}} \quad (2.14)$$

$$\beta = \frac{\omega}{c} \left( \frac{C_d}{C_0} \right) \quad (2.15)$$

$$V_p = C \sqrt{\frac{C_d}{C_0}} \quad (2.16)$$

At higher frequencies however, the above approximations lose accuracy as conductor thickness,  $t$ , substrate height,  $h$ , and line width,  $W$ , begin to have a noticeable effect on the line parameters. Curve fitting techniques have been employed to develop more accurate formulations to somewhat mitigate these higher frequency effects. Nevertheless, this approach is useful for hand calculations in determining line parameters approximately. Full wave electromagnetic analysis methods have become the standard nowadays due to the widespread availability of powerful computers as well as full wave electromagnetic software packages. These techniques solve Maxwell's equations, using advanced numerical methods, for the corresponding line parameters by applying the given boundary conditions. While taking into consideration all longitudinal field components as well, these calculations are usually performed over a number of frequencies and therefore are able to account for dispersive effects of the line. All in all, the full wave analysis techniques are able to provide significantly more accurate results by exploiting modern computing power. Microstrip lines have relatively high loss arising from conductor loss, dielectric loss and radiation loss. Out of these three loss mechanisms, the conductor and dielectric

loss are the most significant. Conductors dissipate power as heat due to the finite conductance of the metal trace. Conductor loss is exacerbated at high frequencies due to the skin effect . At RF and microwave frequencies, current is no longer uniformly distributed across the cross section of the signal trace. Due to eddy currents induced within the trace, signal current vanishes in the centre of the conductor and concentrates near the trace edges. This effectively reduces the cross-sectional area of the trace at high frequencies, increases the trace resistance and therefore also the attenuation constant of the line. Dielectric loss is due to two factors. Firstly, real dielectrics have non-zero conductivity Therefore, the movement of charge between the two conductors via the dielectric is one source of energy loss. Atomic and molecular resonances and the heating effect brought on as a consequence is the second source of dielectric loss. Dielectric loss grows at a much greater rate with frequency than conductor loss and becomes a major concern at higher frequencies. Radiation loss on the other hand is caused by radiating fields inducing currents on other conducting bodies in the vicinity of the line. Although the attenuation constant may be determined with accuracy given the exact knowledge of the trace geometry as well as the field distribution[25] , the computation is complicated. On the other hand, methods such as the perturbation method [26] and Wheel’s incremental inductance formula [5], given by (2.17), may be used to determine conductor attenuation constant,  $\alpha_c$ , approximately, where  $x$  is the distance into the conductor trace,  $W$  is the trace width and the surface resistance,  $R_s$ , is given by (2.18).

$$\alpha_c = \frac{R_s}{2 Z_0} \frac{dZ_0}{\sqrt{\frac{\mu_0}{\epsilon}} dx} \quad (2.17)$$

$$R_s = \sqrt{\frac{\omega \mu_0}{2\sigma}} \quad (2.18)$$

With the widespread availability of full wave electromagnetic software, it is possible to extract the attenuation constants from a matched line, one at a time, from simulations using equation (2.19b), which may be arrived at by the simple manipulation of (2.19a), where in both equations, the magnitude of  $S_{21}$  is used rather than its decibel equivalent.

$$| S_{21} | = e^{-\left(\frac{\alpha_c}{\alpha_d}\right)^z} \quad (2.19a)$$

$$\frac{\alpha_c}{d} = -\frac{\ln | S_{21} |}{z} \quad (2.19b)$$

For example, when the conductor attenuation constant is to be determined, the condition that  $\tan \delta = 0$  is imposed and to determine the dielectric attenuation constant, the metal conductivity,  $\sigma$ , is assumed to be infinite. The overall attenuation constant may be found by the summation of these different attenuation constants. The net attenuation is required to determine the unloaded quality factors of distributed resonators as described in the next section.

## 2.6. Unloaded Quality Factor

The unloaded quality factor of a resonator is a crucial parameter which determines the feasibility of that resonator for filter implementation. Power dissipation within a resonator is inversely proportional to its unloaded quality factor. An ideal resonator having an infinitely large quality factor will not dissipate any power. In contrast, power dissipation, and therefore filter passband insertion loss increases as the unloaded quality factor lowers. Moreover, finite quality factors cause the rounding of passband edges leading to an overall reduction in filter selectivity. Limitations in quality factor are especially a concern in high order filters since the amount of loss incurred as well as the reduction in selectivity are proportional to the number of dissipative resonators employed. A relatively accurate formula (2.20) for estimating the mid-band insertion loss,  $L_i$ , from the unloaded quality factor of the  $i^{\text{th}}$  resonator,  $Q_{ui}$ , and Fractional BandWidth, FBW, and filter order,  $N$ , is described in , where  $g_i$  are the lowpass prototype element values.

$$L_i = 4.343 \sum_{i=1}^N \frac{g_i}{\text{FBW} Q_{ui}} \quad (2.20)$$

Consequently, for the same unloaded quality factor, the mid-band insertion loss will increase for smaller fractional bandwidths as illustrated in Fig.13.a. Likewise, from

Fig.13.b for the same fractional bandwidth, it is seen that the mid-band insertion loss increases with lowering unloaded quality factor. It is also evident from Fig.13.c that there is greater mid band loss for higher filter orders due to the use of more dissipative resonators. In passive lumped element filters, finite quality factors arise mainly due to the winding resistance of the inductors. However, in distributed filters, finite resonator quality factors result largely from the loss a signal incurs as it propagates along the transmission medium. In the case of a microstrip medium, conductor and dielectric loss may be considered the most significant contributors towards loss. Although these losses may be controlled to a certain extent by employing low loss substrates, better conducting traces and resonator topologies less prone to loss, the maximum realistically achievable unloaded resonator quality factors are generally under 300 for copper based microstrip lines.

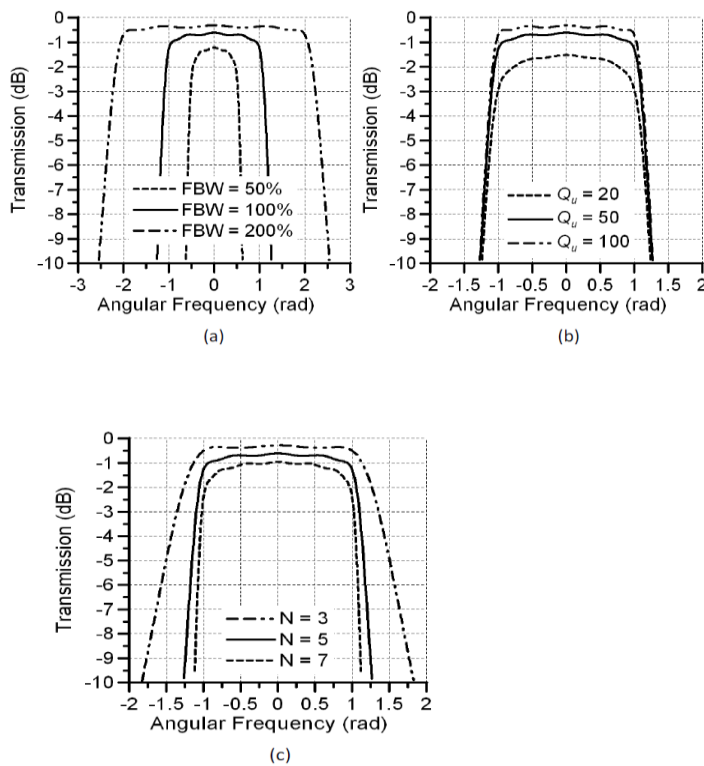


Figure 13: Transmission of normalized Chebyshev bandpass filter. Filter transmission against (a) FBW, where  $Q_u = 50$  and  $N = 5$  (b)  $Q_u$ , where FBW = 100 % and  $N = 5$  (c)  $N$ , where  $Q_u = 50$  and FBW = 100 %

The attenuation constant is required to estimate the unloaded quality factor of a microstrip resonator. To gain insight, Figure 14 plots the unloaded resonator quality

factor of half wavelength microstrip resonators with a resonant frequency of 5 GHz, constructed on typical a high frequency material, against various strip impedances. The attenuation constants extracted from (2.19b) were used to calculate the unloaded quality factors of the resonators. Reducing the strip thickness not only increases the characteristic impedance of the resonator but also increases losses due to the skin resistance. Therefore, the resonator unloaded quality factor degrades with rising strip impedance. The significance of this effect can be seen in Fig.14, where a dramatic reduction of the quality factor can be observed.

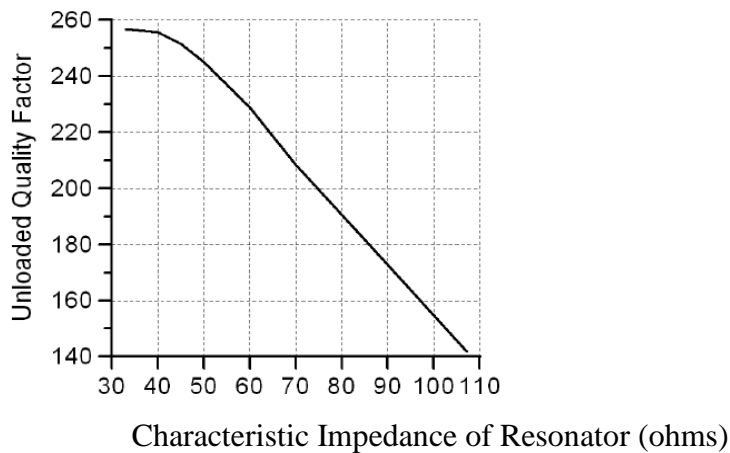


Figure 14: Unloaded Q factor of microstrip  $\lambda/2$  resonator for various characteristic impedances ,where substrate = Rogers 6010LM with  $\epsilon_r = 10.2$ ,  $h = 1.27$  mm with copper conductors.

Since all practical resonators have some degree of internal loss, the resulting filters always exhibit non-zero mid-band insertion loss as well as reduced selectivity. An obvious solution to both these effects is to somehow achieve infinite unloaded quality factor. Intuitively, this implies having resonators with zero loss, which is practically impossible for passive resonators. In effect, if a negative resistance, which exactly cancels that of the resonator, is introduced, zero loss can be achieved. An active device incorporated into a resonator to compensate for its losses is able to do just this and an infinite unloaded quality factor may indeed be attained[20] . However, as with most solutions, there are tradeoffs. Active devices increase power consumption, introduce distortion components, degrade signal to noise ratio and greatly increases circuit complexity and size. From Fig.13.b, it is evident that a slight

increase in the mid-band insertion loss of a lossy filter can not only produce a flatter passband but also improve the filter selectivity. A solution derived from this principle, widely known as lossy filter synthesis, avoids the use of active devices altogether. Lossy elements cause the poles and zeros of a filter to shift slightly to the left in the S-domain. If all resonators have uniform unloaded quality factor, then the shift is by an amount

$\alpha = \omega_o/Q_u$ . The principle behind lossy synthesis is to predistort the original filter poles and zeros so as to compensate for these shifts. For an all-pole filter, while this involves translating the poles to the right, care must be taken to ensure that these are strictly confined to the left half of the S-plane. Fig.15 below illustrates the effect of loss on an ideal filter response and how predistortion to some degree mitigates the reduction in bandwidth and flattens the passband. Although predistorted filters are unable to compensate for the losses as in active filters, a purely passive implementation guarantees that there is no added design complexity.

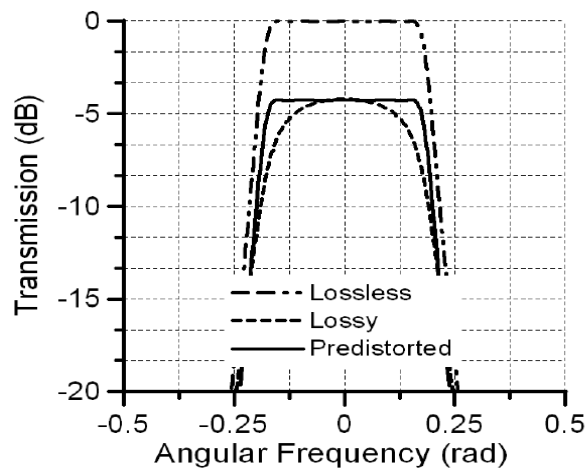


Figure 15: Comparison of 5<sup>th</sup> order Chebyshev filter transmission response for lossless, lossy and predistorted cases (where  $Q_u = 10$  for lossy and predistorted responses).

## 2.7. Microstrip Coupled Lines

A pair of parallel microstrip lines, in close proximity, allows a microwave signal to couple from one line to another. As such, these so called coupled microstrip lines serve as basic building blocks of microstrip filters, where they are employed in

coupling resonators. The cross section of a coupled microstrip line with the corresponding electromagnetic fields in the even and odd mode is illustrated in Fig.16.

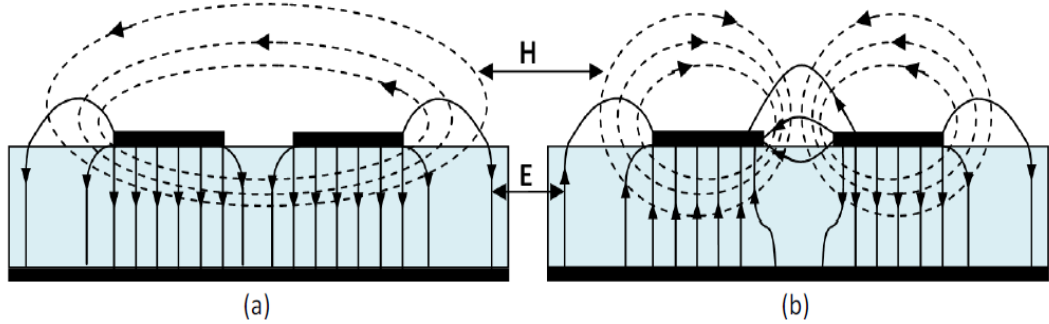


Figure 16: Side on view of field distribution of microstrip coupled lines of (a) even mode (b) odd mode excitation.

Generally, any voltage or current excitation on the lines may be decomposed into even and odd components. In the even mode, signal coupling occurs via the magnetic field and in the odd mode this occurs via the electric field. Although in the general case, both types of field contribute towards coupling, they may interact in either a constructive or destructive manner depending on how the lines are excited. Therefore, the coupling strength observed is in fact due to an interaction of these two effects. In microstrip coupled lines, due to the different field distributions, the even and odd mode propagate at slightly different phase velocities. A lumped element model for a differential element of a pair of coupled transmission lines is illustrated in Fig.5, where  $L_1$ ,  $C_1$ ,  $L_2$  and  $C_2$  are the self inductance and shunt capacitance per unit length of line 1 and line 2 respectively and  $L_m$  and  $C_m$  are the mutual inductance and capacitance per unit length between the two lines. The terminal voltages and currents in general are described by the differential equations (2.21)-(2.24).

$$\frac{dv_1}{dz} = L_1 \frac{dl_1}{dt} + L_m \frac{dl_2}{dt} \quad (2.21)$$

$$\frac{dv_2}{dz} = L_m \frac{dl_1}{dt} + L_2 \frac{dl_2}{dt} \quad (2.22)$$



$$\frac{dl_2}{dz} = C_{1g} \frac{dv_1}{dt} + C_m \frac{d(v_2 - v_1)}{dt} \quad (2.23)$$

$$\frac{dl_1}{dz} = C_m \frac{d(v_1 - v_2)}{dt} + C_{2g} \frac{dv_2}{dt} \quad (2.24)$$

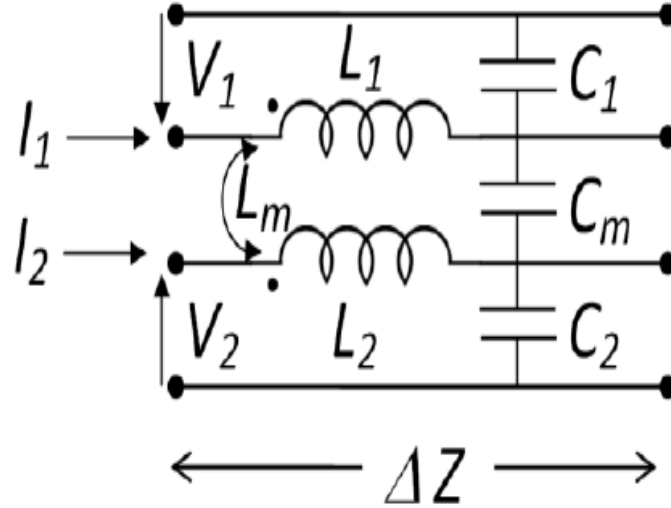


Figure 17: Lumped element circuit model of coupled transmission lines

For an even mode excitation, the terminal voltages  $V_1 = V_2 = V$  and currents  $I_1 = I_2 = I$  are assumed. Applying these conditions to the above equations give (2.25)-(2.28), where  $c_1 = c_{1g} + c_m$  and  $c_2 = c_{2g} + c_m$  are the self capacitances per unit length of the lines 1 and 2 respectively.

$$\frac{dv}{dz} = L_1 \frac{dl}{dt} + L_m \frac{dl}{dt} = (L_1 + L_m) \frac{dl}{dt} \quad (2.25)$$

$$\frac{dv}{dz} = L_m \frac{dl}{dt} + L_2 \frac{dl}{dt} = (L_2 + L_m) \frac{dl}{dt} \quad (2.26)$$

$$\frac{dl}{dz} = C_{1g} \frac{dv}{dt} = (C_1 - C_m) \frac{dv}{dt} \quad (2.27)$$

$$\frac{dl}{dz} = C_{2g} \frac{dv}{dt} = (C_2 - C_m) \frac{dv}{dt} \quad (2.28)$$

The equations below indicate that the even mode equivalent inductance is  $L_1 + L_m$  and  $L_1 - L_m$  while the corresponding capacitance is  $C_1 - C_m$  and  $C_2 - C_m$  for line 1 and 2 respectively. Therefore, the even mode characteristic impedance of line 1 may be defined by (2.29) and the corresponding impedance of line 2 may be similarly defined.

$$Z_{\text{even}} = \sqrt{\frac{L_1 + L_m}{C_1 - C_m}} \quad (2.29)$$

A similar argument for the odd mode where the applied conditions are  $V_1 = -V_2$  and currents  $I_1 = -I_2$  yields the odd mode equivalent inductance as  $L_1 - L_m$  and  $L_2 - L_m$  and corresponding capacitance as  $C_1 + C_m$  and  $C_2 + C_m$  for line 1 and 2 respectively. Therefore, the odd mode characteristic impedance of line 1 may be defined by (2.30) and the corresponding impedance of line 2 may be defined likewise.

$$Z_{\text{odd}} = \sqrt{\frac{L_1 - L_m}{C_1 + C_m}} \quad (2.30)$$

Another key parameter especially for filter design is the coupling coefficient, defined as the ratio of the coupled energy to the stored energy. The normalized electric and magnetic coupling coefficients  $K_E$  and  $K_M$  are given by (2.31) and (2.32) respectively.

$$K_E = \frac{C_m}{\sqrt{C_1 C_2}} \quad (2.31)$$

$$K_M = \frac{L_m}{\sqrt{L_1 L_2}} \quad (2.32)$$

## CHAPTER 3

### DUAL-MODE SQUARE PATCH RESONATOR

#### 3.1. Miniature Dual-Mode Resonator Filters

Dual-mode resonators have been widely used to realize many RF/microwave filters [24]. A major feature and interest of this type of resonator lies indeed that each of dual-mode resonators can be used as a doubly tuned resonant circuit, and moreover the number of resonators required for a  $n$ -degree filter is decreased by half, resulting in a compact filter arrangement.

#### 3.2. Microstrip Dual-Mode Resonators

For our discussion, let us consider a microstrip square patch resonator represented by a Wheeler's cavity model [25]. The EM fields inside the cavity can be expanded in terms of  $TM_{z_{mno}}$  modes:

$$E_z = \sum_{m=0}^{\infty} \sum_{n=0}^{\infty} \cos\left(\frac{\pi m}{a} x\right) \cos\left(\frac{\pi n}{a} y\right)$$
$$H_x = \left(\frac{j\omega\epsilon_{\text{eff}}}{Kc^2}\right) \left(\frac{\partial E_z}{\partial y}\right), \quad H_y = -\left(\frac{j\omega\epsilon_{\text{eff}}}{Kc^2}\right) \left(\frac{\partial E_z}{\partial x}\right) \quad (3.1)$$
$$Kc^2 = \left(\frac{\pi m}{a}\right)^2 + \left(\frac{\pi n}{a}\right)^2$$

Where  $A_{mn}$  represents the mode amplitude,  $\omega$  is the angular frequency, and  $a$  and  $\epsilon_{\text{eff}}$  are the effective width and permittivity [25]. The resonant frequency of the cavity is given by

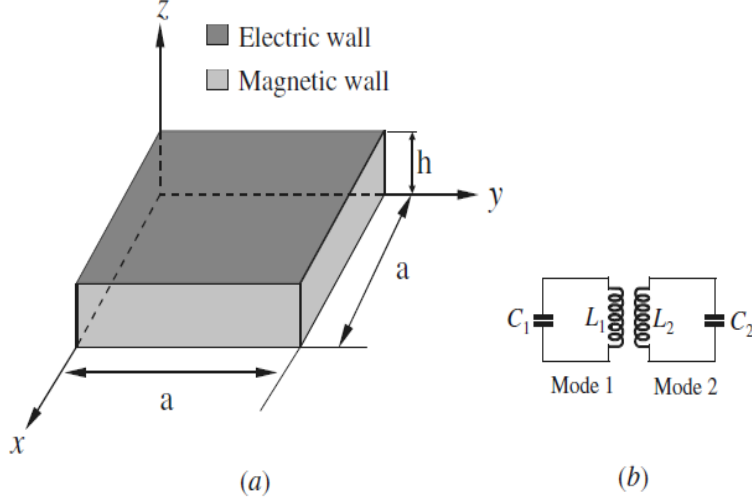


Figure 18: (a) Cavity model of a dual-mode microstrip resonator. (b) Equivalent circuit of the dual-mode resonator.

$$f_{mno} = \frac{1}{2\pi\sqrt{\mu\epsilon_{\text{eff}}}} \sqrt{\left(\frac{m\pi}{a}\right)^2 + \left(\frac{n\pi}{a}\right)^2} \quad (3.2)$$

Note that there are an infinite number of resonant frequencies corresponding to different field distributions or modes. The modes that have the same resonant frequency are called the degenerate modes. Therefore, the two fundamental modes, i.e.,  $\text{TMz}_{100}$  and  $\text{TMz}_{010}$  modes, are a pair of the degenerate modes because

$$f_{100} = f_{010} = \frac{1}{2a\sqrt{\mu\epsilon_{\text{eff}}}} \quad (3.3)$$

Also note from (3.1) that the field distributions of these two modes are orthogonal to each other. In order to couple them, some perturbation to the symmetry of the cavity is needed, and the two coupled degenerate modes function as two coupled resonators, as depicted in Fig.18.b. A microstrip dual-mode resonator is not necessarily square in shape, but usually has a two-dimensional (2-D) symmetry. Fig.19 shows some

typical microstrip dual-mode resonators, where  $D$  above each resonator indicates its symmetrical dimension, and  $\gamma_{g0}$  is the guided-wavelength at its fundamental resonant frequency in the associated resonator. Note that a small perturbation has been applied to each dual-mode resonator at a location that is assumed at a  $45^\circ$  offset from its two orthogonal modes. For instance, a small notch or a small cut is used to disturb the disk and square patch resonators, while a small patch is added to the ring, square loop, and meander loop resonators, respectively. It should be mentioned that for coupling of the orthogonal modes, the perturbations could also take

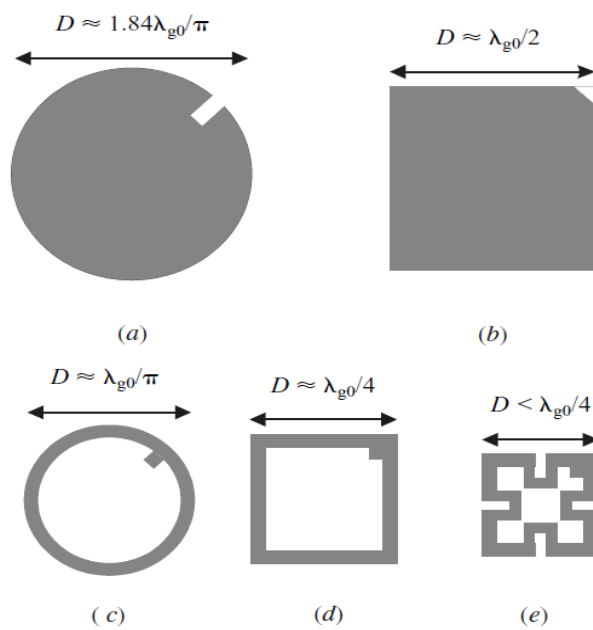


Figure 19: Some microstrip dual-mode resonators. (a) Circular disk. (b) Square patch. (c) Circular ring. (d) Square loop. (e) Meander loop.

forms other than those demonstrated in Figure 19. For example, a small elliptical deformation of a circular patch or disk may be used for coupling the two degenerate modes and, similarly, a square patch may be distorted slightly into a rectangular shape for the coupling.

### 3.2.1. Dual-Mode Resonators

Network synthesis techniques allow the efficient design of a bandpass filter at given specification. The resulting electrical network typically consists of ideal lumped element resonators, which are not practical at RF and microwave frequencies. Therefore an additional step in the development of microwave bandpass filters is the realization of ideal resonators in distributed transmission line media. Distributed resonators however do not behave as their ideal lumped element counterparts since they suffer from limited unloaded quality factor and spurious harmonic resonances. Although virtually all microwave filters are designed around the fundamental resonance of the comprising resonators, spurious passbands are almost always present at integer multiples of the first passband. While a multitude of bandpass filtering functions may be realised by various coupling schemes [26], the particular frequency behavior of the resonator may also be exploited to realize enhanced filters such as those with wider stopbands or multiple passbands. This is especially applicable to distributed resonators since there is usually some degree of control over their frequency behavior. The frequency response of planar resonators may be readily altered by introducing various structural changes for example to shift spurious harmonics outwards [27], introduce additional transmission zeros in the stopband [28][29] or to generate a controllable second passband [30] and [31]. A dual-mode resonator is one that essentially supports two modes of resonance that are non-harmonically related. For planar structures, resonances may occur across both dimensions, namely, the length and width of the transmission lines. For higher frequencies, there may even be resonances across the thickness of the conductor trace. However, not all of these resonances may be readily accessible and tuned. For example, the resonance across the thickness of the conductor can only be varied by altering the thickness of the trace, which is impractical. The term dual-mode in this thesis strictly refers to structures with two modes of resonances that are not only fundamental but are also readily accessible. While  $N$  coupled single-mode resonators are required to realize an  $N$ th order bandpass filter, only  $N/2$  dual-mode resonators are necessary for the same filter since each dual-mode section behaves as a pair of coupled resonators. In addition to potential side reduction, dual mode resonators offer a possibility to reduce overall losses. Although compact dual-mode resonators such as the open-loop [32], circular ring [33], square loop [34] and patch based

resonators [35],[36] have already been proposed, there is still much research interest concerning the development of even more compact structures for filter realization.

### 3.3. Analysis of Dual-Mode Resonator

dual-mode resonator in its most simple form is depicted in Fig. 20, where  $Z_1$  and  $Z_2$  denote characteristic impedances,  $w_1$  and  $w_2$  denote line widths and  $\theta_1$  and  $\theta_2$  are the electrical lengths of the lines. In the absence of the short circuited center stub, the resonator is identical to the single-mode open-loop  $\lambda g/2$  resonator [37]. It will be proved that the inclusion of a short circuited stub along the symmetry plane effectively converts the single-mode resonator to a dual-mode resonator. The grounded stub is relatively short and therefore variations of this resonator may be obtained by folding the longer lines of length  $\theta_1$ . Although not illustrated in Fig.20, the resonator may be coupled to the input and output ports via a direct connection, by parallel coupling or through capacitive coupling.

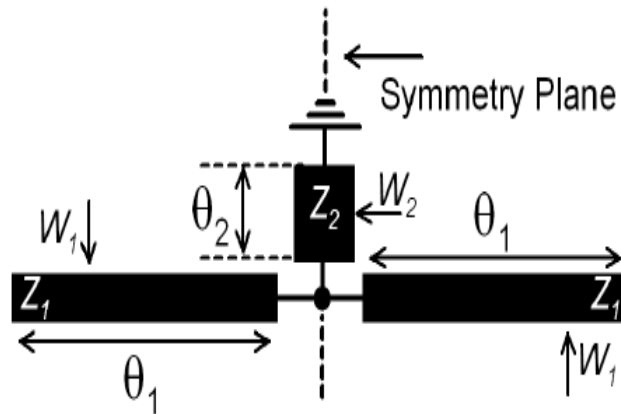


Figure 20: Basic layout of dual-mode resonator

Every excitation driving an electrical network can be separated into even and odd mode components and the overall response is obtained from the superposition of the two. The independence of the two modes permits circuit analysis to be carried out independently for each mode. The analysis of symmetrical networks in particular, such as that in Fig.20, is greatly simplified from this method since complex circuits may be decomposed in to simpler structures. Therefore, a detailed analysis of the

dual-mode resonator performed by even and odd mode decomposition can be found in the following sub sections.

### 3.3.1. Analysis of Odd Mode

The odd mode assumes an asymmetric excitation at the input and output ports and consequently enforces a virtual short circuit in the symmetry plane of the resonator. The short circuited stub, with characteristic impedance  $Z_2$ , is bypassed by the virtual short circuit as it appears in parallel to it. Therefore, the odd mode equivalent resonator circuit configuration takes the form of that in Fig. 21.

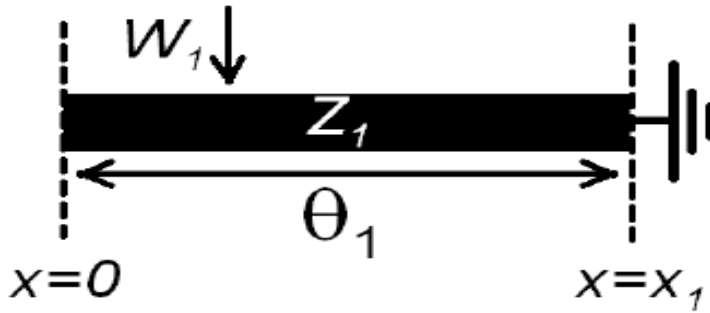


Figure 21: Odd mode resonator configuration

To determine the natural modes of resonance, the following analysis is performed under sinusoidal steady state conditions assuming a loss less line. At any time along a planar transmission line, there may exist a forward and reverse travelling voltage wave and their corresponding current components. The superposition of the forward and reverse components of each type of wave yields the voltage,  $V(x)$ , and current distribution,  $I(x)$ , along the transmission line as given by equations (3.4) and (3.5), where  $v^+$  and  $v^-$  are terms to be determined from the boundary conditions,  $Z_1$  is the characteristic impedance and  $\beta$  is the propagation constant of the line.

$$V(x) = V^+ e^{-j\beta x} + v^- e^{j\beta x} \quad (3.4)$$

$$I(x) = I^+ e^{-j\beta x} - I^- e^{j\beta x} = \frac{v^+}{Z_1} e^{-j\beta x} + \frac{v^-}{Z_1} e^{j\beta x} \quad (3.5)$$



Applying the boundary conditions of the circuit in Fig. 21, which can be summarized as  $V(x_1) = 0$  and  $I(0) = 0$ , to the above equations and solving for the voltage and current distributions gives (3.6) and (3.7).

$$V(x_1) = 2V^+ \text{Cos}[\beta x] \quad (3.6)$$

$$I(x) = -j \frac{2V^+}{Z_1} \text{Sin}[\beta x] \quad (3.7)$$

In order to obtain the modes that may exist on the line, the boundary conditions are enforced on these equations to eliminate  $v^+$  and this leads to the conclusion that any mode which satisfies (3.8) is a natural mode of the odd mode equivalent circuit.

$$\text{Cos}(\beta x) = \cos(\theta_1) \quad (3.8)$$

Solving (3.6) for the natural modes gives infinitely many solutions as given by (3.7), where  $\lambda_g$  is the guided wavelength.

$$\lambda_g = \frac{4x_1}{n} \quad \text{where } n = 1, 3, 5 \dots \dots \quad (3.9)$$

For filter design, only the first resonance mode ( $n = 1$ ) is considered, in which case the electrical length of the transmission line is  $90^\circ$ . The remaining harmonic modes damage the response of a filter as they ultimately produce spurious responses in the stopband. Fig.22.a plots the magnitude of the voltage and current, for the fundamental odd mode ( $n = 1$ ) along the odd mode resonator with normalized length and  $Z_1 = 1$ . The voltage and current distributions along the dual-mode resonator for an odd mode excitation can also be visualized through Fig.22.b and (c) respectively. It is immediately evident from Fig.22.b and (c) that the odd mode experiences a virtual ground in the symmetry plane and is therefore not affected by the short circuited stub. While the voltage standing wave reaches a maximum at both open ends, the current reaches its maximum at the symmetry plane.

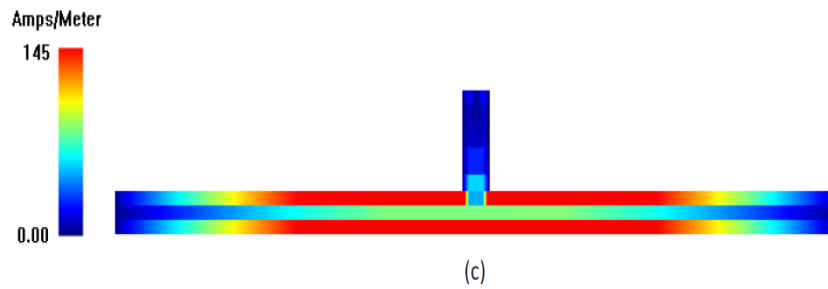
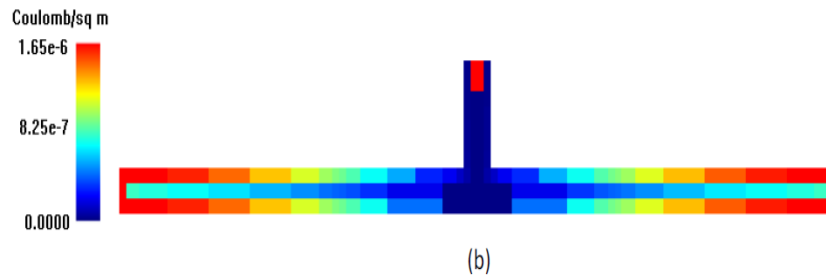
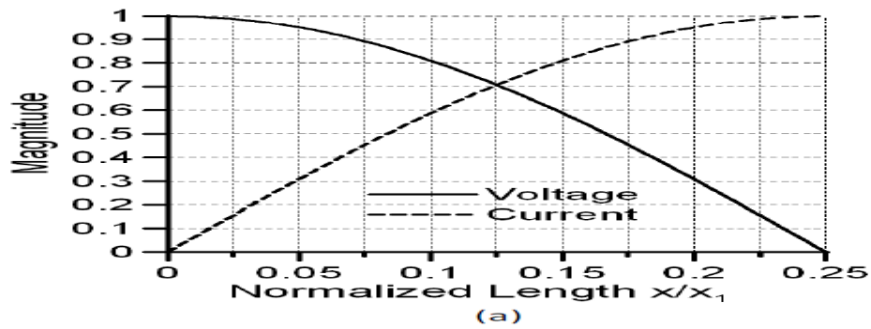


Figure 22: (a) Voltage and current distribution along odd mode resonator normalised to the resonator length, where  $Z_1 = 1$  (b) Full wave EM simulated charge distribution along dualmode resonator (c) Full wave EM simulated current distribution along dual-mode resonator.

### 3.3.2. Analysis of Even Mode

The even mode assumes the symmetrical excitation at the input and output ports and consequently enforces a virtual open circuit in the symmetry plane of the resonator in Fig.23. While this effectively bisects the dual-mode resonator along the symmetry plane, the short circuited stub is split along this plane resulting in an effective characteristic impedance in the even mode to be different to  $Z_2$  and is therefore denoted by  $Z_{2e}$ . The even mode equivalent resonator circuit configuration takes the form of that in Fig. 23.

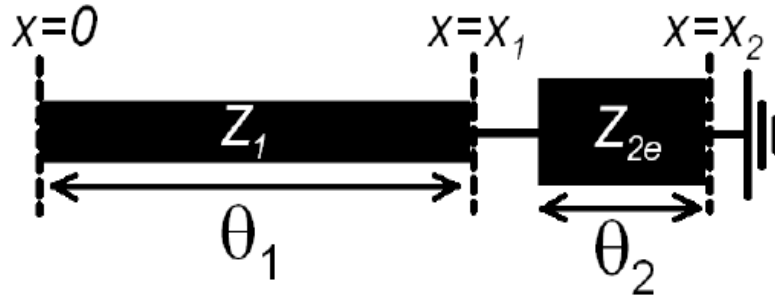


Figure 23: Even mode resonator configuration

Similar to the odd mode, the even mode resonances may be determined from analysing the even mode equivalent resonator under sinusoidal steady state conditions. The even mode resonator is elongated by the short circuited stub. Lower resonant frequencies may therefore be expected for this mode. In order to obtain the voltage and current distributions as well as to quantify the natural modes, the voltage and current for each line will be solved separately and these will be matched at the boundary to obtain the complete solution.

The voltage and current along line 1 can still be expressed by (3.4) and (3.5), and applying the boundary condition  $I(0) = 0$  leads to the corresponding distributions to still take the form of (3.7) and (3.8). Similarly, the voltages and currents along line 2 may be expressed by (3.4) and (3.5), where  $x$  takes values between  $x_1$  and  $x_2$ . After applying the boundary conditions, matching the current and voltage at the  $x = x_1$  boundary and with some manipulations, it is possible to arrive at the voltage and current distributions along the lines as (3.10) and (3.11) respectively.

$$V(x) = \begin{cases} 2V^+ \cos(\beta x), & x < x_1 \\ 2V^+ \frac{\cos(\beta x_1) \sin(\beta(x - x_2))}{\sin(\beta(x_1 - x_2))} & x_1 \leq x \leq x_2 \end{cases} \quad (3.10)$$

$$I(x) = \begin{cases} -j \frac{2V^+}{z_1} \sin(\beta x), & x < x_1 \\ j \frac{2V^+ \cos(\beta x_1)}{z_2 \sin(\beta(x_1 - x_2))} \cos(\beta(x - x_2)), & x_1 \leq x \leq x_2 \end{cases} \quad (3.11)$$

The condition for resonance in the even mode is a transcendental equation (3.12) which must be solved graphically or numerically to obtain the supported guided wavelengths for this mode.

$$\frac{Z_{2e}}{Z_1} \tan(\beta x) \tan[\beta(x_1 - x_2)] - 1 = \frac{Z_{2e}}{Z_1} \tan(\beta \theta_1) \tan(\theta_2) - 1 = 0 \quad (3.12)$$

Fig 24 plots the fundamental guided wavelength, computed from (44), normalized to the fundamental odd mode guided wavelength, against various impedance ratios  $\frac{Z_{2e}}{Z_1}$  and line ratios expressed as a percentage of  $(x_2 - x_1)/x_1$ . It can be seen that as the impedance ratio tends towards unity and the length of line 2 approaches zero, the guided wavelength of the even mode tends towards that of the odd mode. In fact, the split in the resonant frequency between the even and odd mode is exclusively a consequence of the short circuited stub. Essentially, the resonant frequency split increases with stub length and characteristic impedance.

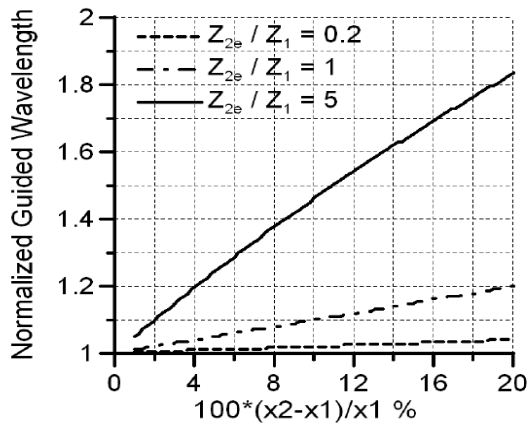
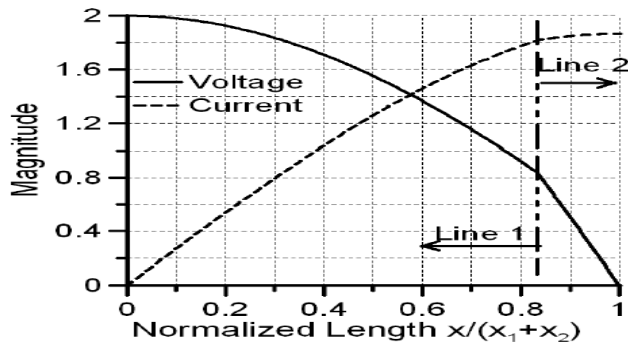


Figure 24: Supported fundamental resonant guided wavelength of even mode, normalized to the first order odd mode guided wavelength, plotted against the length of line 2 expressed as a percentage of that of line 1 for various impedance ratios  $Z_{2e}/Z_1$ .

Fig 25. (a) plots the magnitude of the voltage and current, for the even mode along the even mode resonator with normalized length, where  $Z_1 = 1$  and  $Z_{2e}/Z_1 = 2$ . There is clearly a noticeable difference between the current and voltage on lines 1 and 2 due to the step change in characteristic impedance. This is the first order voltage and current standing wave pattern for the even mode, and from Fig.24, it is evident that the even mode resonance is always at a lower frequency than that of the odd mode. The voltage and current distributions along the dual-mode resonator for an even mode excitation can also be visualized through Fig.25.b , (c) and (d). It is immediately evident from the current distribution in the x direction, as illustrated in Fig.25.c, that there is a virtual open circuit along the symmetry plane of the resonator since there is no x-directed current in the center. The high current density present in both sides of the symmetry plane is in fact diverted to the short circuited stub as is illustrated by the y-directed current density in Figure. 25.d, Similar to the odd mode the voltage standing wave reaches a maximum at both open ends as predicted.



(a)

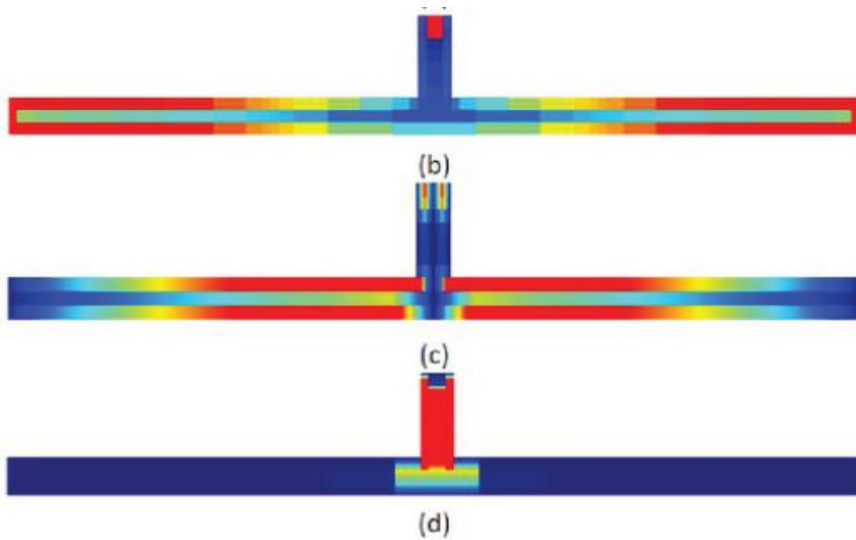


Figure 25: (a) Voltage and current distribution along even mode resonator normalised to the resonator length (b) Full wave EM simulated charge distribution along dual-mode resonator (c) Full wave EM simulated current distribution in the x direction (d) Full wave EM simulated current distribution in the y direction.

### 3.4. Equivalent Electrical Model

The development of an equivalent circuit for the compact dual-mode resonator is a critical step towards not only gaining insight into its electrical behavior but also applying it in filter design. Although the fundamental even and odd mode resonant frequencies were determined from circuit analysis presented in the previous section, knowledge of the resonant frequencies alone is not sufficient for complete characterization. In addition, knowledge of the external quality factor as well as the inter-resonator coupling coefficients are also required. While these parameters are

defined by the physical structure in the distributed dual-mode resonator, the equivalent lumped model, comprising of inductors, capacitors and inverters, will bear the same information within its element values. Due to the presence of two resonant modes, it is assumed that the equivalent circuit would comprise of a pair of synchronously tuned resonators coupled via an immittance inverter. As such, there are two possible circuit implementations of the model as illustrated in Fig. 26 .a and (b). For each model, the parameters, namely, the resonator inductance, capacitance, and inverter immittances must be extracted from the physical structure. To determine the parameters of the first model, the distributed resonator circuit of Fig.20 is redrawn as Fig.26.c, where the impedance looking into the short circuited stub is  $Z_{sc}$ . This configuration allows an impedance inverter of value  $K = |Z_{sc}|$  to be extracted at the symmetry plane of the resonator and this is equated to  $K_2$ , as given by (3.13).

$$K_2 = z_2 \tan(\theta_2) \quad (3.13)$$

The reactance,  $z_{in1}$  given by (3.14), near resonance behaves as a series LC resonator. Applying ,  $z_{in1} = 0$  at resonance yields the resonance condition as (3.15) from which the angular resonant frequency,  $\omega_0$ , may be determined.

$$Z_{in1} = [Z_2 \tan(\theta_2) - Z_1 \cot(\theta_1)] \quad (3.14)$$

$$\tan(\theta_1)\tan(\theta_2) = \frac{Z_1}{Z_2} \quad (3.15)$$

The reactance slope parameter,  $X_r$  , of the series distributed resonator may be derived from (3.13) and is found to be (3.15).

$$X_r = \frac{Z_1 \theta_1 \sec(\theta_1)^2 Z_2 \theta_2 \sec(\theta_2)^2}{2} \quad (3.16)$$

The reactance slope parameter can be used to quantify the series inductance,  $L_s$ , as given by (3.17), from which the series capacitance  $C_s$  may be found from (3.18).

$$L_s = \frac{X_r}{\omega_0} \quad (3.17)$$

$$C_s = \frac{1}{\omega_0^2 L_s} \quad (3.18)$$

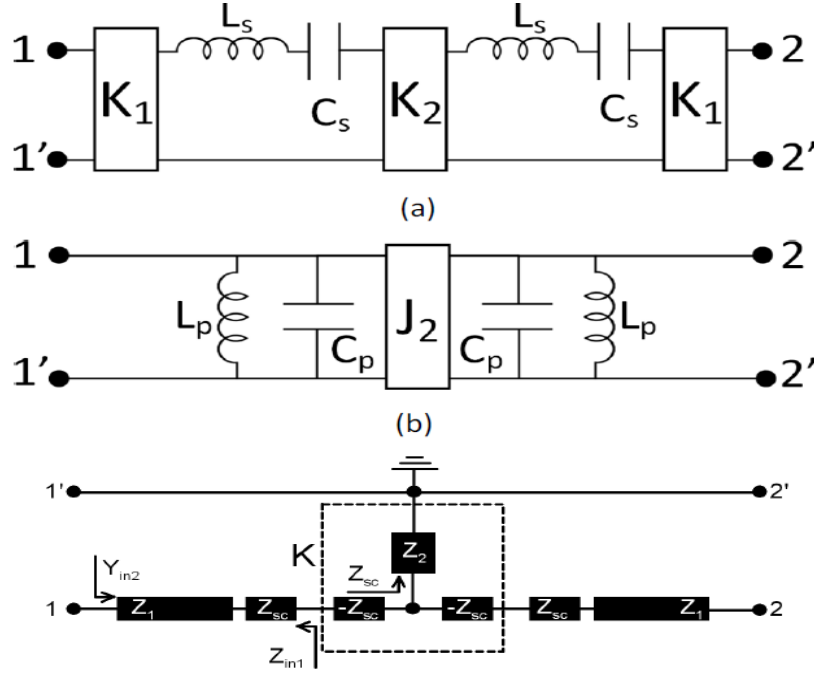


Figure 26: (a) (b) Equivalent circuits of the dual-mode resonator (c) Dual-mode resonator with extracted impedance inverter

The parameters of the second model in Fig 26 (b) may be obtained in a similar fashion by noting that the susceptance,  $Y_{in2}$  given by (3.19), behaves as that of a parallel LC resonant circuit near resonance.

$$Y_{in2} = \frac{1}{z_1} \left( \frac{Z_2 \tan(\theta_1) \tan(\theta_2) - Z_1}{Z_1 \tan(\theta_1) + Z_2 \tan(\theta_2)} \right) \quad (3.19)$$

The resonant condition obtained by imposing  $Y_{in2} = 0$  produces the same result given by (3.19) as expected. The susceptance slop parameter,  $x_s$ , can be derived from the



susceptance as (3.20) from which the resonator capacitance,  $C_p$ , and inductance,  $L_p$ , may be determined from (3.20) and (3.21) respectively.

$$X_s = \frac{z_2}{2z_1} \left( \frac{\theta_1 \sec^2(\theta_1) \tan(\theta_1) + \theta_2 \sec^2(\theta_2) \tan(\theta_2)}{Z_1 \tan(\theta_1) + Z_2 \tan(\theta_2)} \right) \quad (3.20)$$

$$C_p = \frac{X_s}{\omega_0} \quad (3.21)$$

$$L_p = \frac{1}{\omega_0^2 C_p} \quad (3.22)$$

Due to the equivalence of the two models, it is now possible to determine the unknown parameter  $K_1$  and  $J_2$  from the expressions presented above. Since the reactance looking into port 1 of Fig. 26 (a) must match the susceptance looking into port 1 of Fig. 26 (b),  $K_1$  must assume a value given by (3.23).

$$K_1 = \sqrt{\frac{x_r}{x_x}} \quad (3.23)$$

Imposing the condition that the split in the two resonant frequencies must be identical in the two models enables  $J_2$  to be formulated as (3.24).

$$J_2 = \frac{x_r}{K_2 x_s} \quad (3.24)$$

## CHAPTER 4

### DESIGN AND SIMULATION OF SLOTTED PATCH MICROSTRIP BANDPASS FILTER

#### 4.1. Introduction

This chapter is devoted to the design and simulation of miniaturized microstrip dual-mode bandpass filters, realized by using slotted patch resonator. The aim of this chapter is to design and simulate designs of compact to be used in many wireless communication applications with different frequency requirements such as (4.16 GHz and 2.04 GHz). Furthermore, the effects of perturbation patch side length on the resulting filter responses have been evaluated. All filter designs presented in this chapter, have been modeled and simulated using EM simulator package Microwave Office 2009, which performs electromagnetic calculations using the method of moment (MoM) .

#### 4.2. Design and Simulation Results of Slotted Patch Resonator Bandpass Filter

$$\lambda_g = \frac{c}{f_0 \sqrt{\epsilon_{eff}}} \quad (4.1)$$

Where  $\lambda_g$  is guided wavelength,  $c$  light velocity,  $\epsilon_r$  relative dielectric constant,  $f_0$  center frequency and  $\epsilon_{eff}$  effective dielectric constant which can be calculated as [26]:

$$\epsilon_{eff} = \frac{\epsilon_r + 1}{2} + \frac{\epsilon_r - 1}{2} \frac{1}{\sqrt{1 + \frac{12H}{W}}} \quad (4.2)$$

However ,in the present work, effective dielectric constant has been approximated to  $(\epsilon_r + 1)/2$ .

The degree of coupling effect depends on perturbation patch side length which affects resonant frequency of output response[12,26]. On the other hand, the edge spacing between slotted patch resonator and I/O feeders can be properly tuned to maximize return loss and minimize insertion loss to optimize frequency response of the filter. However, extensive details about this subject are to be presented later in this chapter.

#### 4.2.1. Design and Simulation Results of BPF Designed for 4.16 GHz

In this study, a dual-mode microstrip patch bandpass filter structures have been designed at frequency of 4.16 GHz as in Figure (27). It has been supposed that, these filter structures have been etched using a substrate with a dielectric constant of 10.8 and thickness of 1.27 mm. Two 50 ohm feed lines as input and output (I/O) ports are placed in orthogonal manner . Accordingly, the side length of the square slotted patch resonator,  $L = 9$  mm, has been determined as:

$$L = 0.3\lambda_g \quad (4.3) \quad (4.3)$$

The side length of the square slotted patch resonator,  $L = 9$  mm .The perturbation square patch side length (d) is 0.8 mm while the gap between I/O feeders and slotted patch resonator is 0.2 mm. Also, the values of X,Y,Q and S are 3 mm,2 mm,1mm and 0.6 mm respectively . The procedural steps of the suggested microstrip BPF using electromagnetic modeling and simulation have been represented in the flowchart in Figure(28).

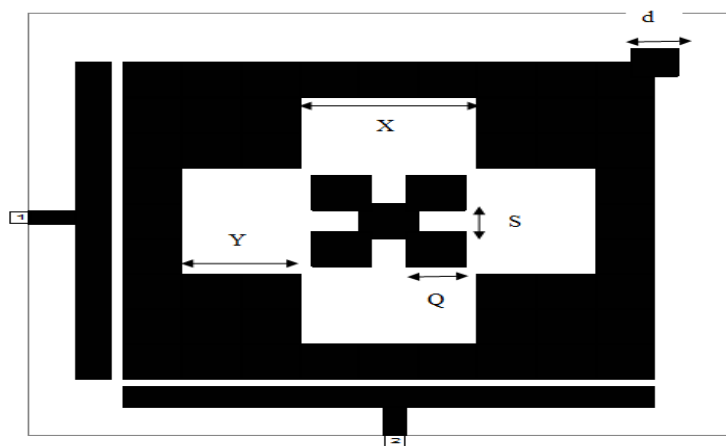


Figure 27: The layout of the modeled dual-mode slotted patch BPF

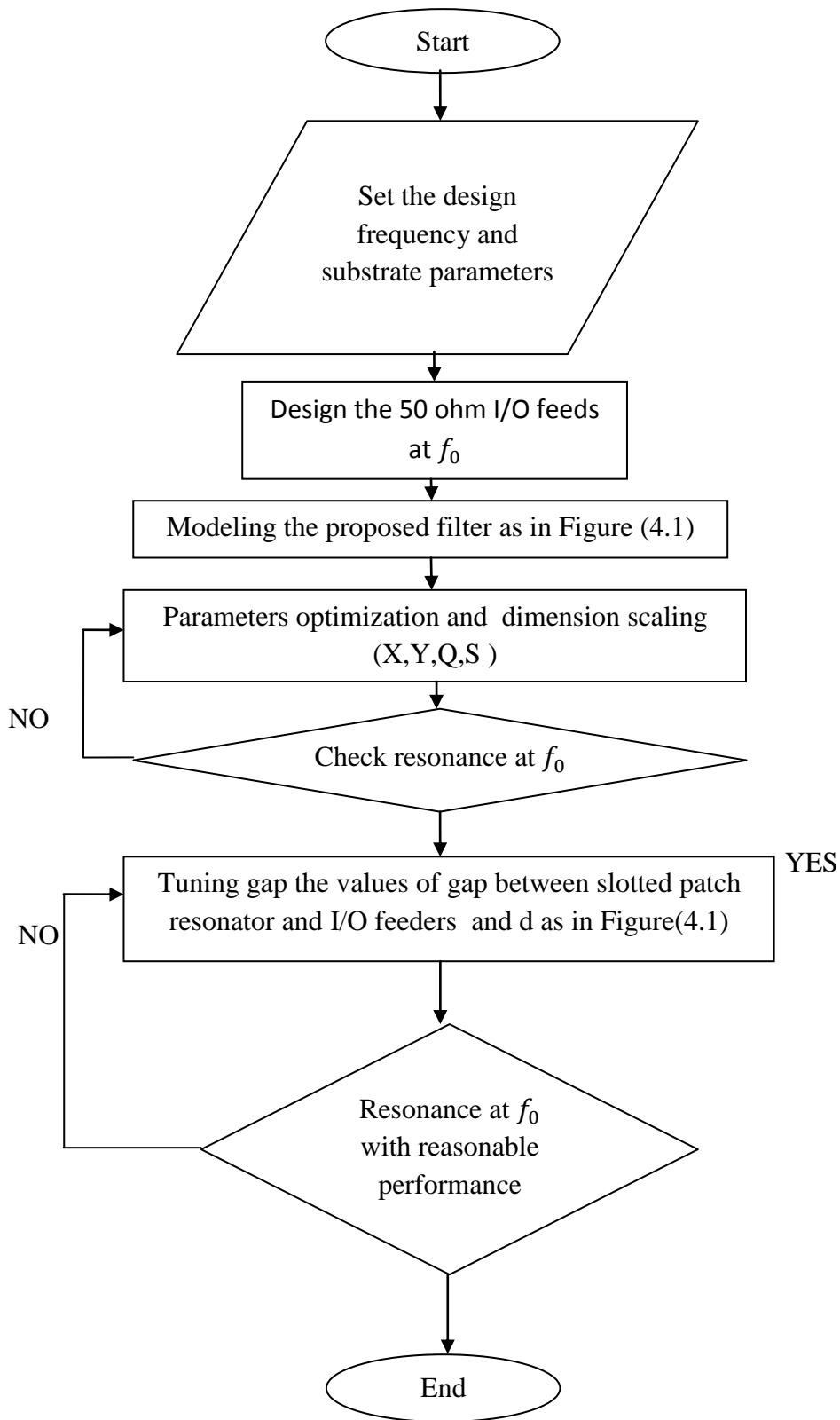


Figure 28: Flow chart for Moore BPF designs

Fig.29 shows the return loss and transmission responses of these filters. Table.1 presents a summary of the modeled filter dimensions as designed for 4.16 GHz applications together with corresponding filter performance parameters. Fig. 30 shows the scattering parameter of the phase response for S11 and S12 with respect to different frequencies. This phase response includes some frequency jumps which are the significant properties of quasi elliptic BPFs

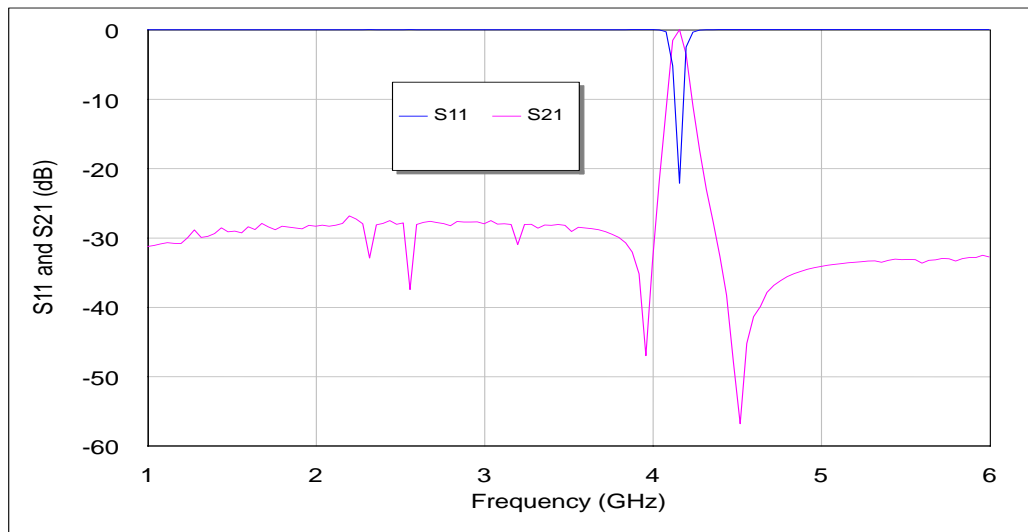


Figure 29: The return loss and transmission responses of proposed BPF designed for 4.16 GHz

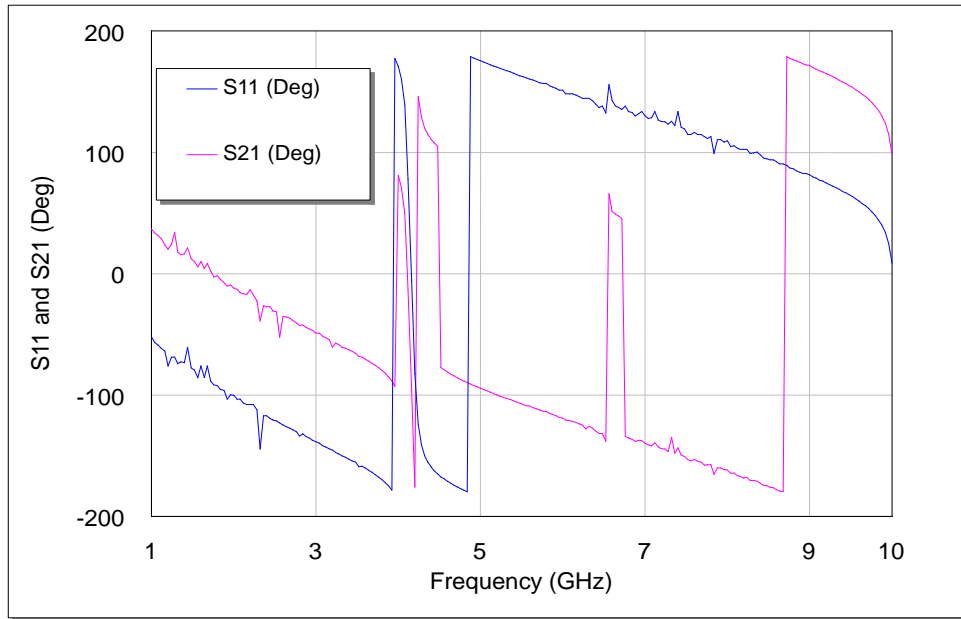


Figure 30: The phase responses of proposed slotted patch BPF

Table 1: Summary of the calculated and simulation results of the modeled filter

<b>Filter Dimensions and Parameters</b>	<b>Magnitude</b>
Occupied Area, mm <sup>2</sup>	96.04
Band Rejection Levels(dB)	-47 (left) -57 (right)
S <sub>11</sub> (dB)	-22.1
Insertion Loss(dB)	-0.03
Bandwidth(MHz)	85

#### 4.2.2. Design And Simulation Results Of BPF Designed For 2.042 and 2.046 GHz Resonant Frequencies

##### GHz Resonant Frequencies

In this case, the bandpass filter structure has been modeled and simulated using the same substrate properties as in Fig.27. This filter has been designed for the resonant frequencies of 2.042 and 2.046 GHz respectively.

Fig.31 show the return loss and transmission responses of this filter. Table 2 presents a summary of the modeled filter dimensions with corresponding filter performance parameters.

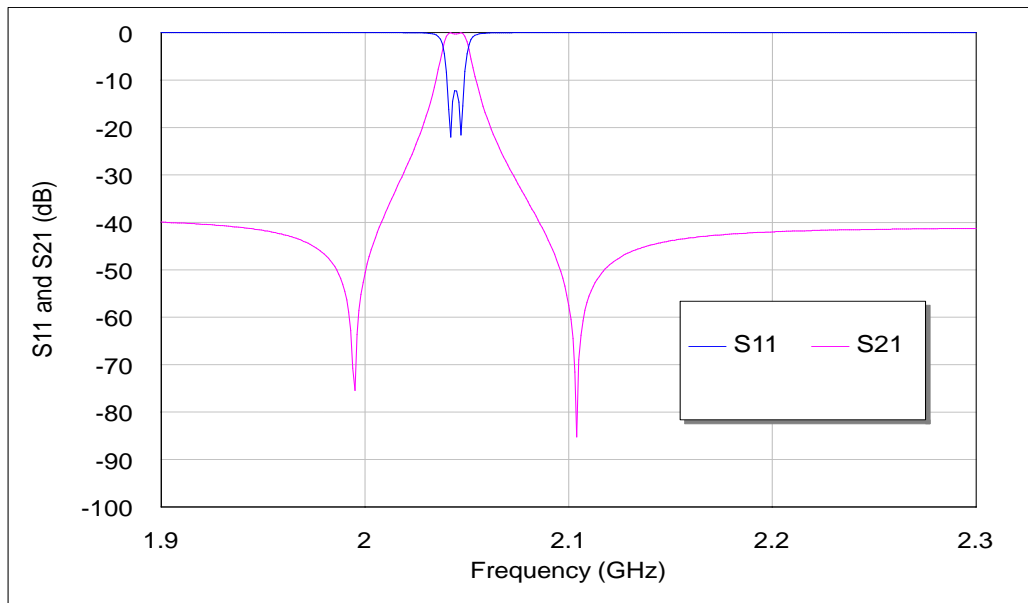


Figure 31: The return loss and transmission responses of proposed BPF designed for 2.04 GHz resonant frequencies

The side length of the square slotted patch resonator,  $L = 18$  mm while the perturbation square patch side length ( $d$ ) is 0.8 mm while the gap between I/O feeders and slotted patch resonator is 0.2 mm. Also, the values of  $X, Y, Q$  and  $S$  are 3 mm, 2 mm, 1 mm and 0.6 mm respectively .

Fig.32 shows phase responses for  $S_{11}$  and  $S_{21}$  with respect to different frequencies .

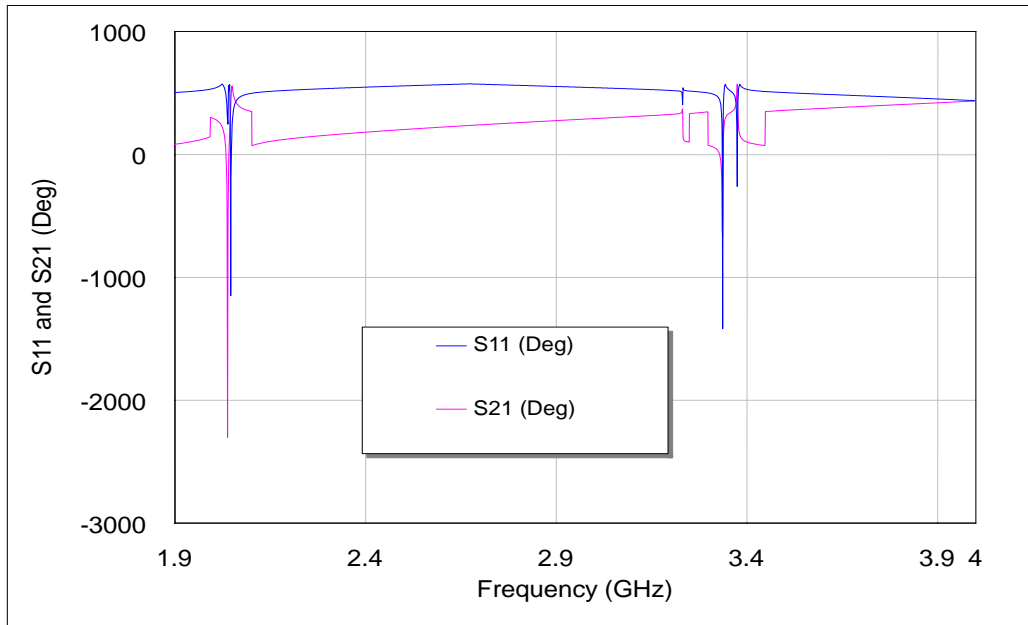


Figure 32: The phase responses of proposed slotted patch BPF



Table 2: Summary of the calculated and simulation results of the modeled filter

<b>Filter Dimensions and Parameters</b>	<b>Magnitude</b>
Occupied Area, mm <sup>2</sup>	376.36
BandRejection Levels(dB)	-75(left) -85(right)
S <sub>11</sub> (dB)	-22
Insertion Loss(dB)	-0.26
Bandwidth(MHz)	11.6

### 4.3. Discussion of the Results

Filter structures, as in Fig.27, has been modeled and analyzed at operating frequencies 4.16 and 2.04 GHz using Microwave Office 2009 electromagnetic simulator from Advanced Wave Research (AWR) Inc. This simulator performs electromagnetic analysis using the method of moments (MoM). The corresponding simulation results of return loss and transmission responses of these filters are shown in Fig.29 and Fig.31, respectively. Results show that the resulting bandpass filters possess good performance curves. As can be seen, all of the filter responses show two transmission zeros rather symmetrically located around the design frequency. Tables 1 and 2 demonstrated the simulated dimensions of the resulting slotted patch microstrip filters. All structures have been designed at the design frequency and using the same substrate material.

Figures 30,32 show the non-linear phase response for S<sub>11</sub> and S<sub>12</sub> with respect to different frequencies. The phase responses in Fig.30 includes higher frequency jumps as compared to Fig.32 which are the significant properties of quasi elliptic BPFs.

Fig.33 illustrates the layout of the dual-mode conventional patch BPF. The use of square slotting principle in conventional patch reduces their fundamental frequency. This is due to the application of surface square cuts which increase the current path length, produce a decrease or shifting in the resonance frequency and transmission

zeros without changing the external dimensions as can be seen from S21 responses depicted in Fig.34 and S11 responses illustrated in Fig.35. This acts as a miniaturization factor in addition to dual mode property because decreasing the fundamental frequency requires more dimension scaling. By the way, the decreased fundamental frequency has been obtained by a slotted patch resonator in accordance with a conventional patch resonator without changing the external dimensions.

One of the most serious problems that degrades the bandpass filter performance is the harmonic. Harmonic frequency is a component frequency of filter response that is an integer multiple of the fundamental frequency, i.e. if the fundamental frequency is  $f$ , the harmonics have frequencies  $2f, 3f, 4f, \dots$  etc.

Fig.36 and Fig.37 show the out-of-band transmission responses of the two filters designed for 4.16 and 2 GHz respectively. It is clear that the performance response does not back up harmonics that conventionally accompany the bandpass filter responses. The 2nd harmonic response appearing in Figure 37 is of little importance, since it is with a very narrow-band and low value of return loss.

Fig.38 and Fig.39 respectively demonstrate surface current density simulation results at 4.16 and 2.04 GHz fundamental frequencies. In these figures, the red color indicates the maximum coupling effect while the blue color indicates the minimum one. The proposed techniques can be generalized as a flexible design tool for compact microstrip bandpass filters for a wide variety of wireless communication systems. Also, the proposed filter designs can be applied to many other wireless communication systems, in this case, the filter dimensions must be scaled up or down depending on the required operating frequencies. For 4.16 and 2.04 GHz design cases, we can see from Figures 40 and 41 that increasing  $d$ , the side length of the small perturbation square patch at the right top corner, causes S21 first to move rapidly upward toward the ideal 0dB point and then split into two visible peaks. Ideally there would be no coupling between the two modes at  $d = 0$  mm.

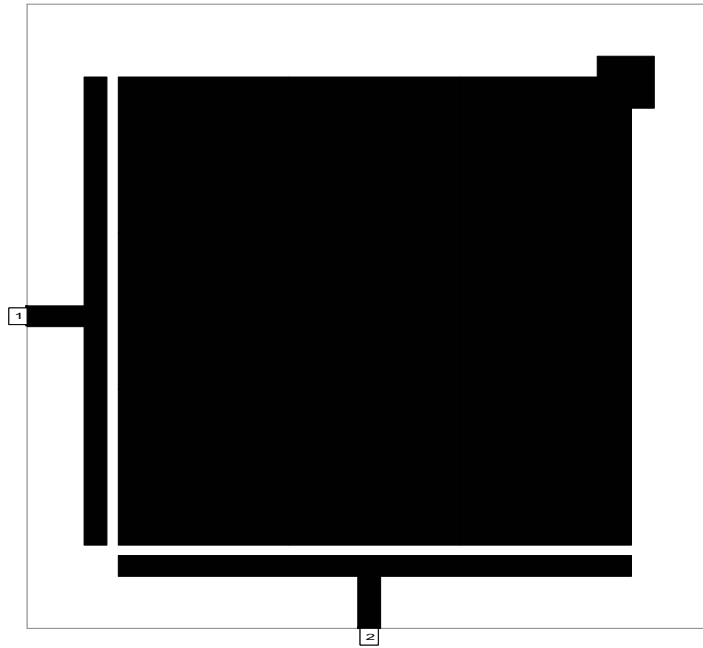


Figure 33: The layout of the modeled dual-mode conventional patch BPF

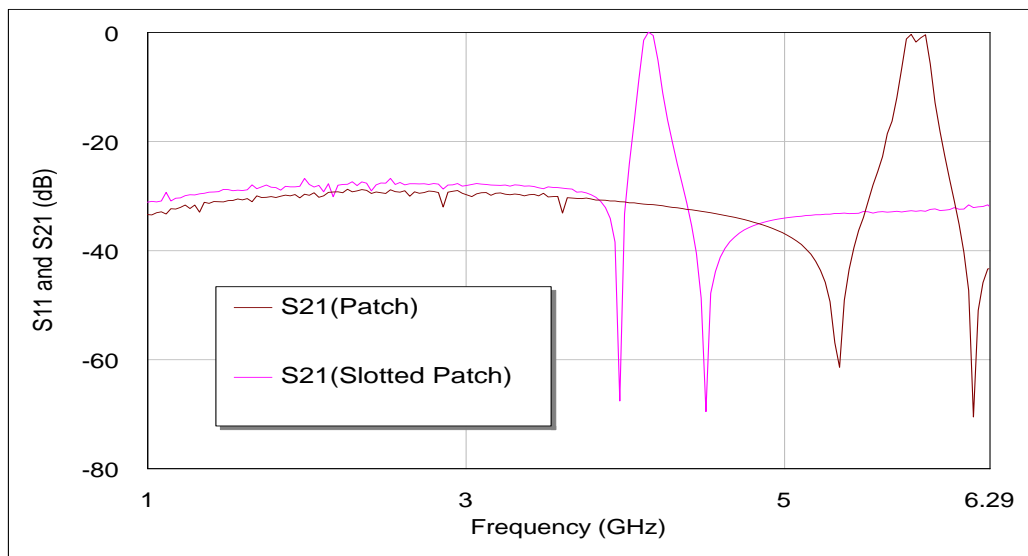


Figure 34: The transmission responses of the two filters; with and without uniform slot at 4.16 and 5.77 GHz respectively

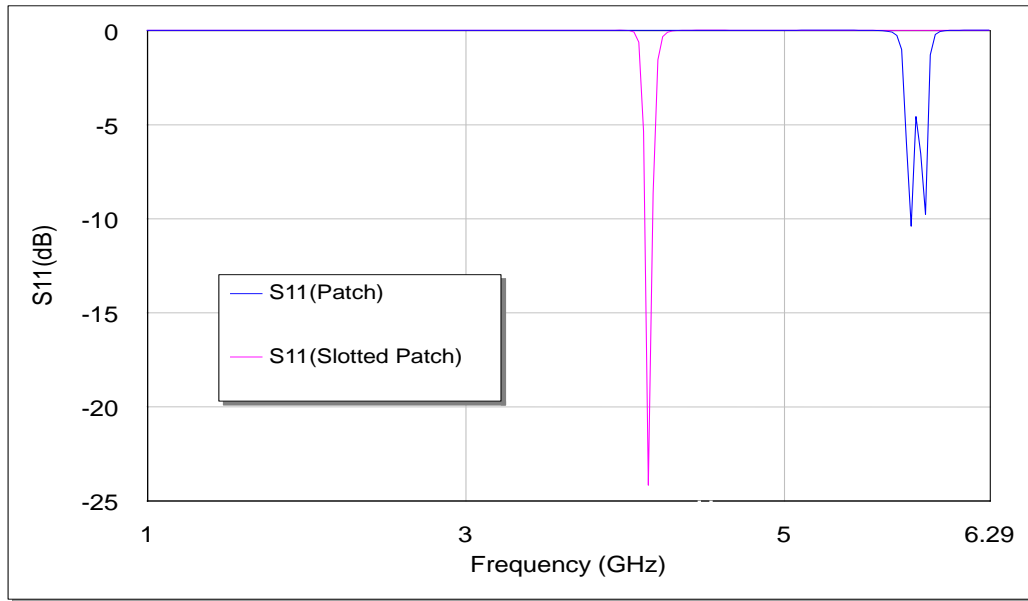


Figure 35: The return loss responses of the two filters; with and without uniform slot at 4.16 and 5.77 GHz respectively

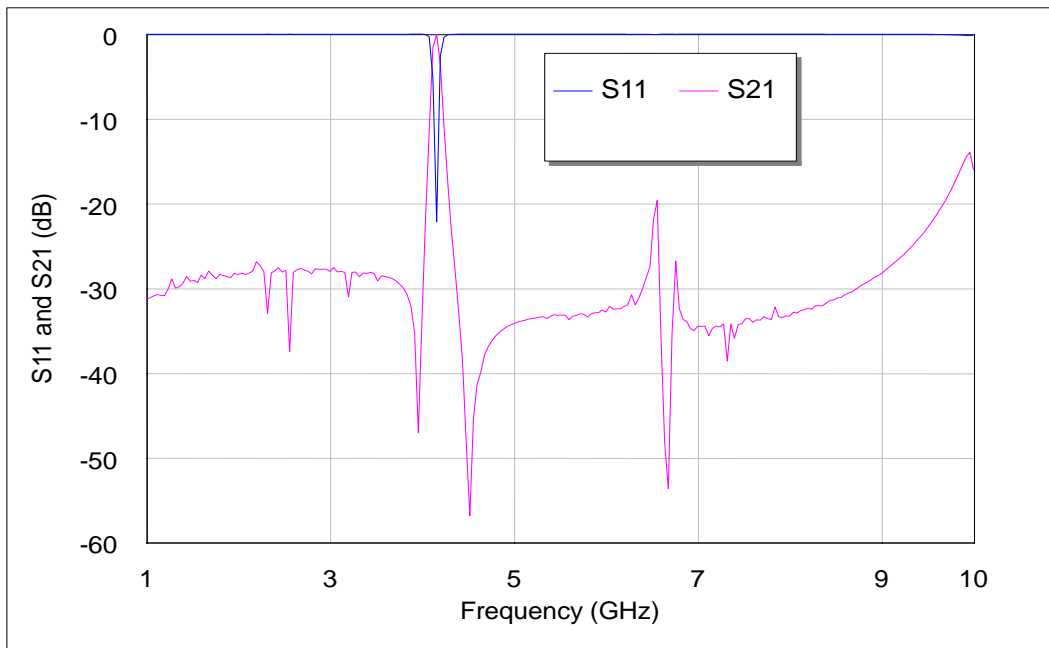


Figure 36: The out-of-band transmission responses of the proposed filter designed for 4.16 GHz fundamental frequency

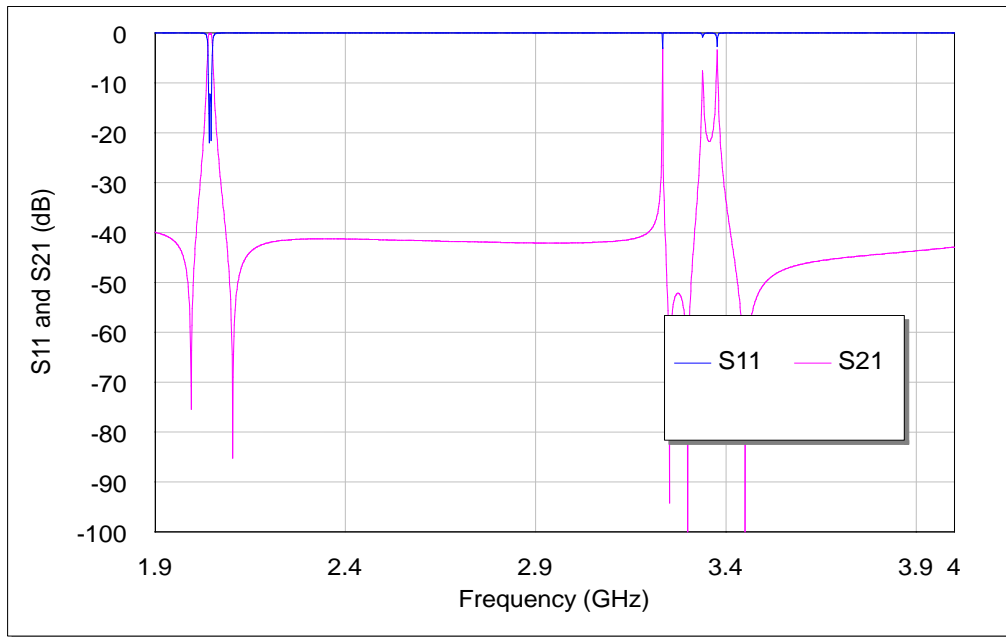


Figure 37: The out-of-band transmission responses of the proposed filter designed for 2.04 GHz fundamental frequency

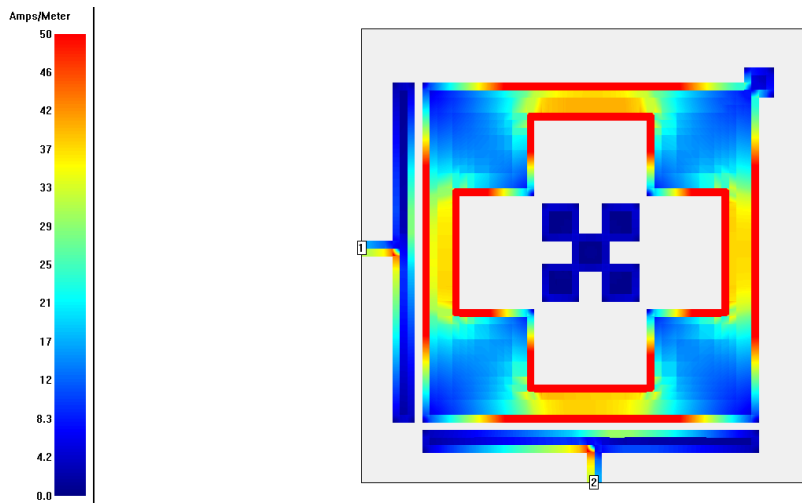


Figure 38: Simulated current density distributions of the proposed BPF at 4.16 GHz fundamental frequency

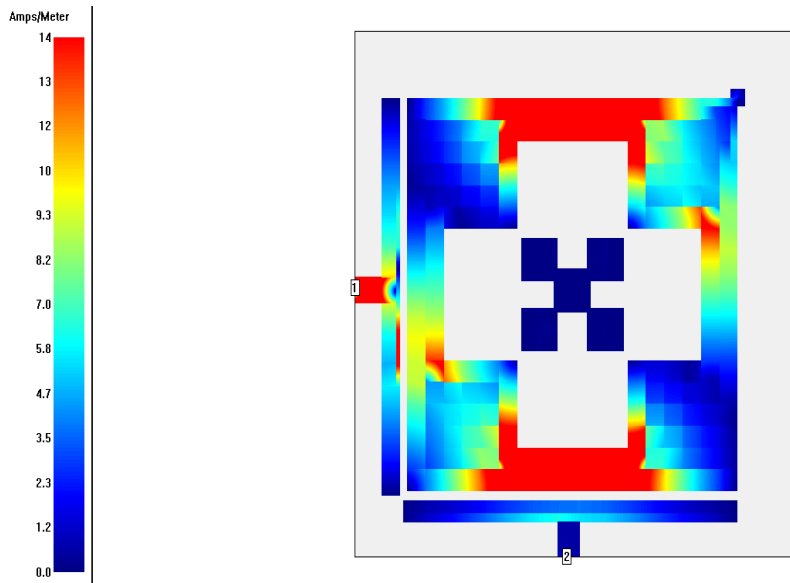


Figure 39: Simulated current density distributions of the proposed BPF at 2.04 GHz fundamental frequency

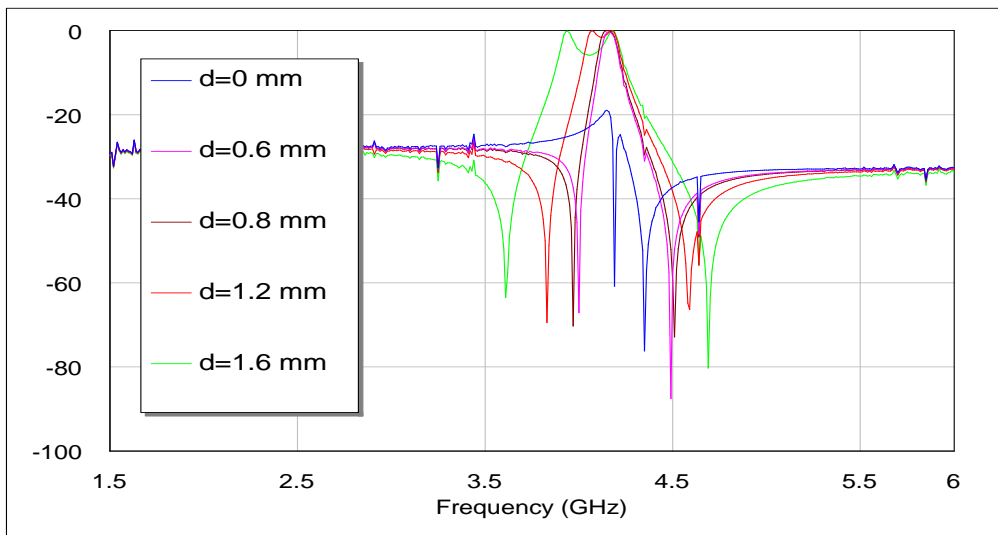


Figure 40: Simulated transmission responses,  $S_{21}$ , of proposed BPF as a function of  $d$  in units of mm for the case of 4.16 GHz

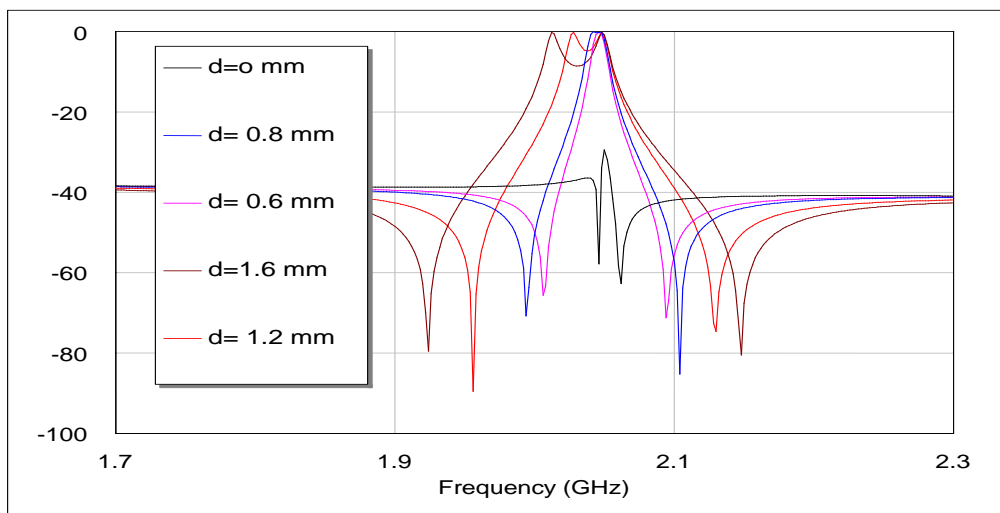


Figure 41: Simulated transmission responses, S21, of proposed BPF as a function of  $d$  in units of mm for the case of 2.04 GHz

## CHAPTER 5

### CONCLUSIONS AND SUGGESTIONS FOR FUTURE WORKS

#### 5.1. Conclusions

A narrowband, compact, and flexible fabricated microstrip bandpass filter design is introduced in this thesis as a candidate for use in modern wireless systems. The proposed filter design is based on the use of dual-mode (two pole) patch microstrip resonator with uniform geometrical slot. This filter has the advantages of possessing much narrower and sharper performance responses as compared to single mode resonator and other conventional square patch filters. The performance of filter structures, based on dual-mode resonators, has been evaluated using Microwave Office Electromagnetic Software Package. Two filters have been designed at resonant frequencies of 4.16 and 2.04 GHz using a substrate with a dielectric constant of 10.8 and thickness of 1.27mm. Performance simulation results show that these filter structures offer very good frequency responses in addition to narrow bands gained, compactness properties and 2<sup>nd</sup> harmonic suppression in out of band region. The application of uniform geometrical slot in conventional patch decreases the fundamental frequency. This is because of the application of surface square cuts which increase the current path length, produce a decrease or shifting in the resonance frequency and transmission zeros without changing the external dimensions .

#### 5.2. Suggestions For Future Works

Microstrip patch bandpass filters have been successively used in many microwave circuits due to their outstanding properties of flexible manufacturing, small sizes and so on. Compact microstrip filters are essential for the next-generation of wireless communication systems, because with the quick expansions of modern communication systems, smaller filters with improved performances are still



requested. Some of the suggestion that can be recommended in this issue can be summarized as follows:

1. Relating the work presented in this thesis, additional works can be done to perform the experimental verifications for modeled designs.
2. Design meander slotted patch resonators to get filters with more enhanced frequency responses and more compact sizes.
3. High Temperature Conductivity (HTC) technique can be used for proposed slotted patch BPFs with very good performance .

## REFERENCES

1. **Lugo C. and Papapolymerou J., (2005)**, "*Bandpass Filter Design Using A Microstrip Triangular Resonator with Dual-Mode Operation*", IEEE Transactions, Microwave and Wireless Components Letters., vol. 15, pp. 475-477.
2. **Hong J. S. and Li S., (2003)**, "*Dual-Mode Microstrip Triangular Patch Resonators and Filters*", IEEE MTT-S Dig., vol. 17, pp. 1901-1904.
3. **Hong J. S. and Li S., (2004)**, "*Theory and Experiment of Dual-Mode Microstrip Triangular-Patch Resonators and Filters*", IEEE Transactions, Microwave Theory Techniques, vol. 52, pp. 1237-1243.
4. **Xiao J. S. and Li Y., (2006)**, "*Novel Planar Bandpass Filters Using Single Patch Resonators with Corner Cuts*", Journal of Electromagnetic Waves and Applications, vol. 20, no.11, pp. 1481-1493.
5. **Wang X. and Li Y., (2003)**, "*Microstrip Bandpass Filter Using One Single Patch Resonator with Two Transmission Zeros*", Electron Letters vol.39, no.17, pp. 1255-1256.
6. **Wasaki A. H., (1996)**, "*A Circularly Polarized Small-Size Microstrip Antenna with A Cross Slot*", IEEE Trans Antennas Propagation, vol. 53, pp. 2087-2098
7. **Hong J. S. and Lancaster M. J., (1995)**, "*Bandpass Characteristics of New Dual-Mode Microstrip Square Loop Resonators*", Electronics Letters , vol.31, no.11, pp. 891- 892.

8. **Chen J. G. and Xue Q., (2005)**, "*Novel Microstrip Bandpass Filter Using One Equilateral Triangular-Patch Resonator*", *Microwave Optic Techniques, Letters*, vol. 44, pp. 222-223.
9. **Tan B. T., (2002)**, "*A Modified Microstrip Circular Patch Resonator Filter*" *IEEE Microwave and Wireless Components Letters*, Vol. 12, pp. 2011-2020.
10. **Wang S. X. and Li Y., (2003)**, "*New Microstrip Triangular Patch Resonators Filters with Two 'Transmission Zeros'*" , *Asia-Pacific Conference on Environmental Electromagnetic*, pp. 364-368.
11. **Akgün H. O. and Görür A., (2004)**, "*Reduced-Size Dual-Mode Slotted Patch Resonator for Low-Loss and Narrowband Bandpass Filter Applications*" ,vol. 40, no. 20. pp. 560-599.
12. **Sheta A. F. and Mohra A., (2006)**, "*Investigation of New Non-Degenerate Dual-Mode Microstrip Patch Filter*", vol. 12, no. 26.
13. **Chen C. H., Lin Y.F., Chen H.M., Yang C. F., and Chou D. W., (2007)**, "*A Miniature Dual-Mode Triangular Patch Band pass Filter Using Al<sub>2</sub>O<sub>3</sub> substrate*", *International Symposium Antenna and Propagation society*, pp. 1-4.
14. **Singh Y. K. and Chakrabarty A., (2008)**, "*Miniaturized Dual-Mode Circular Patch Bandpass Filters With Wide Harmonic Separation*", *Microwave and Wireless Components Letters*, vol. 18, no. 9, pp. 584-586.
15. **Esfeh B. K., (2009)**, "*Narrowband Elliptic Bandpass Filter Using Dual-Mode Microstrip Square Loop Resonator for WiMax Application*", *Modern Applied Science* , vol. 3. no. 9, pp. 2-10.
16. **Yuan C. Li. and Xue Q., (2011)**, "*Dual-Mode Dual-Band Bandpass Filter Based on a Stub-Loaded Patch Resonator*", *IEEE Microwave and Wireless Components Letters* , vol. 21, no. 10, pp. 525-527.

17. **Zhang R. and Zhu L., (2012)**, *“Microstrip Bandpass Filters Using Triple-Mode Patch-Loaded Cross Resonator”*, Progress In Electromagnetic Research Letters, vol. 30, pp. 13-19.
18. **Zhang R., Zhu L. and Luo S., (2013)**, *“Design Methodology of a Class of Triple-Mode Bandpass Filters Using a Patch-Loaded Cross Resonator”*, IEEE International Symposium Wireless (IWS), pp.1-4.
19. **Liua X. and Shib X., (2014)**, *“New Dual-Mode Square Patch Bandpass Filter Using CSRR Slot-Type Perturbation”*, Optic International Journal for Light and Electron Optics, pp.1-4.
20. **Krupka J., Geyer R. G., Kuhn M. and Hinken J. H., (1994)**, *“Dielectric Properties of Single Crystals of Al<sub>2</sub>O<sub>3</sub>, LaAlO<sub>3</sub>, NdGaO<sub>3</sub>, SrTiO<sub>3</sub> and MgO at cryogenic temperatures”*, IEEE Transactions. MTT-42, Oct. Trans. MTT-42.
21. **Pramanick P. and Bhartia P., (1985)**, *“Computer-Aided Design Models for Millimeter-Wave Fin Lines and Suspend-Substrate Microstrip Lines”*, IEEE Transactions, MTT-33, PP. 1429–1435.
22. **Hong J. S. and Lancaster M. J., (2001)**, *“Microstrip Filters for RF/Microwave Applications”*, New York: John Wiley & Sons, 2001.
23. **Hong J. S. and Lancaster M. J., (1997)**, *“Theory and Experiment of Novel Microstrip Slow-Wave Open-Loop Resonator Filters”*, IEEE Transactions on Microwave Theory and Techniques, vol. 45, no. 12, pp. 2358-2365.
24. **Kai P. H., Meng H. K., Weng T. K. and Martins R. P., (2004)**, *“A Compact Microstrip  $g/4$ -SIR Inter Digital Bandpass Filter with Extended Stopband”*, IEEE ,Int. Microwave Symposium. pp. 1621- 1624.

25. **Griol A., Marti J. and Sempere L., (2001)**, *“Microstrip Multistage Coupled Ring Bandpass Filters Using Spur-Line Filters for Harmonic Oppression”*, Electronics Letters, vol. 37, no. 9, pp. 572-573.
26. **Mondal P. and Mandal M. K., (2008)**, *“Design of Dual-Band bandpass Filters Using Stub-Loaded Open-Loop Resonators”*, IEEE Transactions on Microwave Theory and Techniques, vol. 56, no.1, pp. 150-155.
27. **Ping Y. and Sun M.,(2006)**, *“Dual-Band Microstrip Bandpass Filter Using Stepped-Impedance Resonators with New Coupling Schemes”*, IEEE Transactions on Microwave Theory and Techniques, vol. 54, no. 10, pp. 3779-3785.
28. **Hong J. S. Shaman H., and Chun Y. H., (2007)**, *“Dual-Mode Microstrip Open-Loop Resonators and Filters”*, IEEE Transactions on Microwave Theory and Techniques, vol. 55, no. 8, pp. 1764-1770.
29. **Kundu A. C. and Awai I., (2001)**, *“Control of Attenuation Pole Frequency of A Dual-mode Microstrip Ring Resonator Bandpass Filter ”*, IEEE Transactions on Microwave Theory and Techniques, vol. 49, no.6, pp. 1113-1117.
30. **Hong J. S. and Lancaster M. J., (1995)**, *“Realization of Quasielliptic Function Filter Using Dual Mode Microstrip Square Loop Resonators”*, Electronic Letters, vol. 31, no. 24, pp. 2085-2086.
31. **Hong J. S. and Li S., (2004)**, *“Theory and Experiment of Dual-Mode Microstrip Triangular Patch Resonators and Filters ”*, IEEE Transactions on Microwave Theory and Techniques, vol. 52, no. 4, pp. 1237-1243.
32. **Mirshekar S. D. and Davies J. B., (1979)**, *“Accurate Solution of Microstrip and Coplanar Structures for Dispersion and for Dielectric and Conductor Losses”*, IEEE Transactions on Microwave Theory and Techniques, vol. 27, no. 7, pp. 694 – 699.

33. **Athukorala L. and Budimir D., (2010)**, "*Design of Compact Dual-Mode Microstrip Filters*", IEEE Transactions on Microwave Theory and Techniques, vol. 58, no. 11, pp. 2888-2895.
34. **Hong J. S. and Lancaster M. J., (1997)**, "*Theory and Experiment of Novel Microstrip Slow-Wave Open-Loop Resonator Filters*", IEEE Transactions on Microwave Theory and Techniques , vol. 45, no. 12, pp. 2358-2365.
35. **Pozar D. M., (2004)**, "*Microwave Engineering, 3<sup>rd</sup> Edition*", New York: John Wiley & Sons.
36. **Chang C. Y. and Itoh T., (1990)**, "*Microwave Active Filters based on Coupled Negative Resistance Method*", IEEE Transactions on Microwave Theory and Techniques, vol. 38, no. 12, pp. 924- 927.
37. **Tu W. H. and Chang K., (2005)**, "*Miniaturized Dual-Mode Bandpass Filter with Harmonic Control*", IEEE Microwave and Wireless Component Letters, vol. 15, no. 12, pp. 838-840.

## APPENDIX

### CURRICULUM VITAE

#### PERSONAL INFORMATION

**Surname, Name:** Coran, Ali Najdet Nasret

**Nationality:** Iraqi

**Date and Place of Birth:** 30 December 1985, Bagdad

**Marital status:** Single

**Phone:** 05380775296

**Mail:** ali\_hjk2000@yahoo.com

#### EDUCATION

Degree	Institution	Year of Graduation
MSc.	Çankaya Univ. Electronics and Communication Engineering	2014
BSc.	AL-Mustansiriyah. Univ. Electronics and Communication Engineering	2010

#### FOREIGN LANGUAGES

Turkish, Arabic, English